

*ARMY RESEARCH LABORATORY*



## **Low-Level Turbulence Forecasts From Fine-Scale Models**

**by Jeffrey E. Passner**

**ARL-TR-6847**

**February 2014**

## **NOTICES**

### **Disclaimers**

The findings in this report are not to be construed as an official Department of the Army position unless so designated by other authorized documents.

Citation of manufacturer's or trade names does not constitute an official endorsement or approval of the use thereof.

Destroy this report when it is no longer needed. Do not return it to the originator.

# **Army Research Laboratory**

White Sands Missile Range, NM 88002-5501

---

---

**ARL-TR-6847**

**February 2014**

---

## **Low-Level Turbulence Forecasts From Fine-Scale Models**

**Jeffrey E. Passner**

**Computational and Information Sciences Directorate, ARL**

REPORT DOCUMENTATION PAGE			Form Approved OMB No. 0704-0188		
<p>Public reporting burden for this collection of information is estimated to average 1 hour per response, including the time for reviewing instructions, searching existing data sources, gathering and maintaining the data needed, and completing and reviewing the collection information. Send comments regarding this burden estimate or any other aspect of this collection of information, including suggestions for reducing the burden, to Department of Defense, Washington Headquarters Services, Directorate for Information Operations and Reports (0704-0188), 1215 Jefferson Davis Highway, Suite 1204, Arlington, VA 22202-4302. Respondents should be aware that notwithstanding any other provision of law, no person shall be subject to any penalty for failing to comply with a collection of information if it does not display a currently valid OMB control number.</p> <p><b>PLEASE DO NOT RETURN YOUR FORM TO THE ABOVE ADDRESS.</b></p>					
1. REPORT DATE (DD-MM-YYYY) February 2014		2. REPORT TYPE Final		3. DATES COVERED (From - To) 2/2012–1/2014	
4. TITLE AND SUBTITLE Low-Level Turbulence Forecasts From Fine-Scale Models			5a. CONTRACT NUMBER		
			5b. GRANT NUMBER		
			5c. PROGRAM ELEMENT NUMBER		
6. AUTHOR(S) Jeffrey E. Passner			5d. PROJECT NUMBER		
			5e. TASK NUMBER		
			5f. WORK UNIT NUMBER		
7. PERFORMING ORGANIZATION NAME(S) AND ADDRESS(ES) U.S. Army Research Laboratory Computational and Information Sciences Directorate Battlefield Environment Division (ATTN: RDRL-CIE-M) White Sands Missile Range, NM 88002-5501			8. PERFORMING ORGANIZATION REPORT NUMBER ARL-TR-6847		
9. SPONSORING/MONITORING AGENCY NAME(S) AND ADDRESS(ES)			10. SPONSOR/MONITOR'S ACRONYM(S)		
			11. SPONSOR/MONITOR'S REPORT NUMBER(S)		
12. DISTRIBUTION/AVAILABILITY STATEMENT Approved for public release; distribution is unlimited.					
13. SUPPLEMENTARY NOTES					
14. ABSTRACT: <p>Research conducted by the U.S. Army Research Laboratory's (ARL's) Battlefield Environment Division (BED) has been identified as helpful to the Air Force Weather Agency's capability gaps in forecasting boundary-layer and low-level clear-air turbulence (CAT). It was determined that ARL would research, test, and validate low-level turbulence prediction techniques using the Advanced Research version of the Weather Research and Forecasting (WRF) Model (WRF-ARW). The WRF-ARW is a mesoscale weather prediction system designed to serve both operational and forecasting needs. The initial part of this study included a literature search and scientific coordination with other researchers to understand low-level turbulence forecasting techniques, algorithms, and indices. Five methods were selected to test using output from ARL's 1-km study over the Los Angeles domain and the U.S. Air Force Weather Agency's (AFWA's) 1.67-km domain over several areas with high airport traffic to use as verification. Upon completion of the model runs, basic statistical methods were applied to evaluate the forecast usefulness. A final step was to find the strengths of weaknesses of the techniques selected to see which methods were most useful for small-scale turbulence forecasts, what adjustments might be needed, and the direction of future research in this area.</p>					
15. SUBJECT TERMS: mesoscale, WRF, evaluation, turbulence, model					
16. SECURITY CLASSIFICATION OF:			17. LIMITATION OF ABSTRACT  UU	18. NUMBER OF PAGES  60	19a. NAME OF RESPONSIBLE PERSON Jeffrey E. Passner
a. REPORT Unclassified	b. ABSTRACT Unclassified	c. THIS PAGE Unclassified			19b. TELEPHONE NUMBER (Include area code) (575) 678-3193

Standard Form 298 (Rev. 8/98)  
Prescribed by ANSI Std. Z39.18

---

## Contents

---

<b>List of Figures</b>	<b>iv</b>
<b>List of Tables</b>	<b>vi</b>
<b>1. Summary</b>	<b>1</b>
<b>2. Introduction</b>	<b>1</b>
<b>3. The WRF</b>	<b>2</b>
<b>4. Turbulence Evaluation</b>	<b>4</b>
4.1 Techniques to Solve Turbulence .....	4
4.2 ARL Turbulence .....	4
4.3 AFWA Turbulence .....	7
4.4 McCann’s Boundary-Layer Turbulence (BLTURB) Method .....	7
4.5. Unified Post Processor Turbulence .....	8
4.6 Explicit TKE Predicted by the WRF .....	9
<b>5. Turbulence Evaluation</b>	<b>9</b>
5.1 Case of 13 May 2013 in the Northeast USA—Instability and Turbulence .....	19
5.2 Convective Turbulence and Outflow .....	26
5.3 Strong Down Slope Winds: 19 December 2012 .....	32
<b>6. Discussion</b>	<b>35</b>
<b>7. Conclusions</b>	<b>44</b>
<b>8. References</b>	<b>46</b>
<b>List of Symbols, Abbreviations, and Acronyms</b>	<b>49</b>
<b>Distribution List</b>	<b>51</b>

---

## List of Figures

---

Figure 1. Domains 1, 2, 3 (9, 3, and 1-km grid spacing) centered over southern California for this experiment.....	3
Figure 2. The upper-air observation from Edwards Air Force Base at 1500 UTC on 16 February 2012. ....	13
Figure 3. A 500-hPa upper-air map with height, temperature, and winds for 1200 UTC on 16 February 2012. ....	14
Figure 4. ARL turbulence forecast method at 1600 UTC for level 10 on 16 February 2012.....	15
Figure 5. AFWA turbulence forecast method at 1600 UTC for level 10 on 16 February 2012. ....	16
Figure 6. UPP turbulence forecast method at 1600 UTC for level 10 on 16 February 2012. ....	17
Figure 7. BLTURB forecast method for turbulence at 1600 UTC at level 10 on 16 February 2012.....	18
Figure 8. MYJ PBL TKE forecast method for turbulence at 1600 UTC on level 10 on 16 February 2012. ....	19
Figure 9. At 1200 UTC on 13 May 2013, upper-air observation at Upton, NY.....	20
Figure 10. At 1200 UTC on 13 May 2013, 500-hPa heights.....	21
Figure 11. Satellite photo from 1645 UTC on 13 May 2013.....	21
Figure 12. Turbulence forecast at 1700 UTC on 13 May 2013 using the ARL forecasting routine at level 22.....	22
Figure 13. WRF forecasted wind speed at 915-m AGL at 1700 UTC on 13 May 2013 for level 22.....	23
Figure 14. Vertical profile of RH (percent) forecasted for 1700 UTC at location 40.8° N 74.6° W on 13 May 2013.....	24
Figure 15. Vertical profile of qcloud (kg/kg) forecasted for 1700 UTC at location 40.8° N 74.6° W on 13 May 2013.....	24
Figure 16. Vertical Profile of W (m/s) forecasted at 1700 UTC at location 40.8° N 74.6° W on 13 May 2013. ....	25
Figure 17. Upper-air observation at Santa Teresa, NM (EPZ) at 0000 UTC on 21 June 2013.....	26
Figure 18. Radar image at 2326 UTC on 20 June 2013 from Santa Teresa, NM.....	27
Figure 19. WRF 1.67-km forecast for surface winds at 2300 UTC on 20 June 2013. ....	28
Figure 20. Turbulence forecast from AFWA routine at 26-m AGL (Level 2) for 20 June 2013 using WRF 1.67-km output over LRU grid. ....	29
Figure 21. Santa Teresa, NM (EPZ) radar at 0200 UTC on 2 July 2013.....	30
Figure 22. Santa Teresa, NM radar at 0259 UTC 2 July 2013. ....	30

Figure 23. WRF 1.67-km surface wind forecast with terrain data at 0300 UTC on 2 July 2013.....	31
Figure 24. ARL turbulence forecast using WRF output at 0300 UTC on 2 July 2013. ....	32
Figure 25. The 1200 UTC on 19 December 2012 sounding at EPZ.....	33
Figure 26. At 1500 UTC 1.67-km WRF surface wind forecast for 19 Dec 2012 over the LRU/WSMR grid.....	34
Figure 27. ARL forecast for turbulence using the 1.67-km WRF at 1500 UTC on 19 December 2012 over the Las Cruces/WSMR grid. ....	35
Figure 28. On 7 April 2011, the 1500 UTC plot of 1-km WRF winds and forecasted turbulence using the ARL routine at level 9, which is the approximate level of where the Aerostat was flying. The red dot is at a location where one of the Aerostats was lost.....	37
Figure 29. On 7 April 2011, the 1600 UTC plot of 1-km WRF winds and forecasted turbulence using the ARL routine at level 9, which is the approximate level of where the Aerostat was flying. ....	38
Figure 30. On 7 April 2011, the 1700 UTC plot of 1-km WRF winds and forecasted turbulence using the ARL routine at level 9, which is the approximate level of where the Aerostat was flying. ....	39
Figure 31. On 7 April 2011, the 1800 UTC plot of 1-km WRF winds and forecasted turbulence using the ARL routine at level 9, which is the approximate level of where the Aerostat was flying. ....	40
Figure 32. On 7 April 2011, the 1600 UTC plot of 1-km WRF-derived MYJ TKE at level 9, which is the approximate level of where the Aerostat was flying. ....	41
Figure 33. On 7 February 2011, the 1900 UTC (level 7) 1-km turbulence forecast with FDDA included. Elevation (m) is plotted in the contoured over the domain. ....	43
Figure 34. On 7 February 2011, 1900 UTC plot (level 7) of 1-km turbulence forecast without FDDA Elevation (m) is plotted in contours over the domain. ....	44

---

## List of Tables

---

Table 1. Criteria for turbulence intensity used by ARL.....	7
Table 2. Criteria for turbulence and intensity used by AFWA. ....	7
Table 3. Criteria for turbulence and intensity used by the BLTURB. ....	8
Table 4. Criteria for turbulence and intensity used by the UPP.....	9
Table 5. “YES/NO” turbulence forecasts for the five days studied.....	10
Table 6. Turbulence intensities from the ARL routine. The number of forecasts in each group is the vertical total and the number of observations in each group is the horizontal total.....	10
Table 7. Turbulence intensities from the UPP routine. For each group the number of forecasts is the vertical total and the number of observations is the horizontal total.....	11
Table 8. Turbulence intensities from the AFWA routine. For each group the number of forecasts is the vertical total and the number of observations is the horizontal total. ....	11
Table 9. Turbulence intensities from the BLTURB routine. For each group the number of forecasts is the vertical total and the number of observations is the horizontal total. ....	11
Table 10. Observations from 1300 to 1600 UTC on 7 April 2011 at FOB Dwyer, Afganistan 31.10° N 64.08° E (725-m elevation). ....	40

---

## 1. Summary

---

Research conducted by the U.S. Army Research Laboratory's (ARL's) Battlefield Environment Division (BED) has been identified as helpful to the U.S. Air Force Weather Agency's (AFWA's) capability gaps in forecasting boundary-layer and low-level clear-air turbulence (CAT). It was determined that ARL would research, test, and validate low-level turbulence prediction techniques using the Advanced Research version of the Weather Research and Forecasting (WRF) Model (WRF-ARW). The WRF-ARW is a mesoscale weather prediction system designed to serve both operational and forecasting needs. The initial part of this study included a literature search and scientific coordination with other researchers to understand low-level turbulence forecasting techniques, algorithms, and indices. Five methods were selected to test using output from ARL's 1-km study over the Los Angeles domain and the AFWA's 1.67-km domain over several areas with high airport traffic to use as verification. Upon completion of the model runs, basic statistical methods were applied to evaluate the forecast usefulness. A final step was to find the strengths of weaknesses of the techniques selected to see which methods were most useful for small-scale turbulence forecasts, what adjustments might be needed, and the direction of future research in this area.

---

## 2. Introduction

---

An aerostat is an aircraft that remains aloft primarily through the use of light gases. The structure of the aerostat consists of an envelope that contains a lightweight skin that provides a lifting gas that makes the aircraft buoyant and allows other components to be attached (1). Aerostats are kept in place with a mooring system that works like a fishing rod. The tether, usually made of Kevlar, is the line, and the moor, which is either mobile or immobile, works like the rod. The aerostat has electrical conductors in and it is also equipped with fiber optic cables, making it responsible for getting the data from the payload down to the crew on the ground (2).

The harsh weather conditions of Afghanistan have led to ongoing losses in the aerostat fleet. In February 2013 alone, there were 10 major incidents out of 99 systems. The February 2013 mishaps compare with four major incidents in February 2012, when there were 86 aerostats in theater, and four incidents in February 2011, when there were 46 aerostats on hand. Six of the incidents in February 2013 involved aerostats that "crashed due to wind." Strong winds, powerful downdrafts, lightning, rain, and even snow are damaging or destroying so many of the aircraft, that in 2011, the Central Command, which runs the war in Afghanistan, analyzed aerostat mishaps in an attempt to derive ways to prevent them (3).

Upon completion of the statistical evaluation, the methods were evaluated to see which ones or what combination of the methods could be used to improve small-scale turbulence forecasts. Additionally, model strengths and weaknesses were studied for future studies to improve forecasting skill at small scales.

---

### **3. The WRF**

---

The WRF V3.4.1 was used in this study (4). To resolve the local terrain features, a triple-nested configuration was adopted for the model. The nests were centered at a location at  $32.9^{\circ}$  N and  $117.1^{\circ}$  W, as shown in figure 1. The outer domain was  $175 \times 175$  in horizontal dimensionality, while domain 2 had  $241 \times 241$  and domain 3 had  $127 \times 127$ , respectively. Additionally, the WRF was run with 57 terrain-following vertical sigma layers. The model was integrated from 1200 to 1200 Coordinated Universal Time (UTC) for five case days from early 2012 over the southwestern United States. However, turbulence forecasts were examined only on 16 February, 1 March, and 5 March. The case days were chosen to include more benign weather. A significant turbulence event occurred over southern California on 16 February with more quiescent weather observed on 1 March and 5 March. The observation nudging capability of WRF (5) can be used to incorporate observations into the model via a 6-h pre-forecast (1200 to 1800 UTC). However, for this initial part of the study (using the southern California study area) turbulence forecasts were compared to Pilot Reports (PIREPs) without using observational nudging in the forecast. The WRF model was run on the Army's High-Performance Computing Research Center Linux Network Evolocity II, which is a cluster system (6).

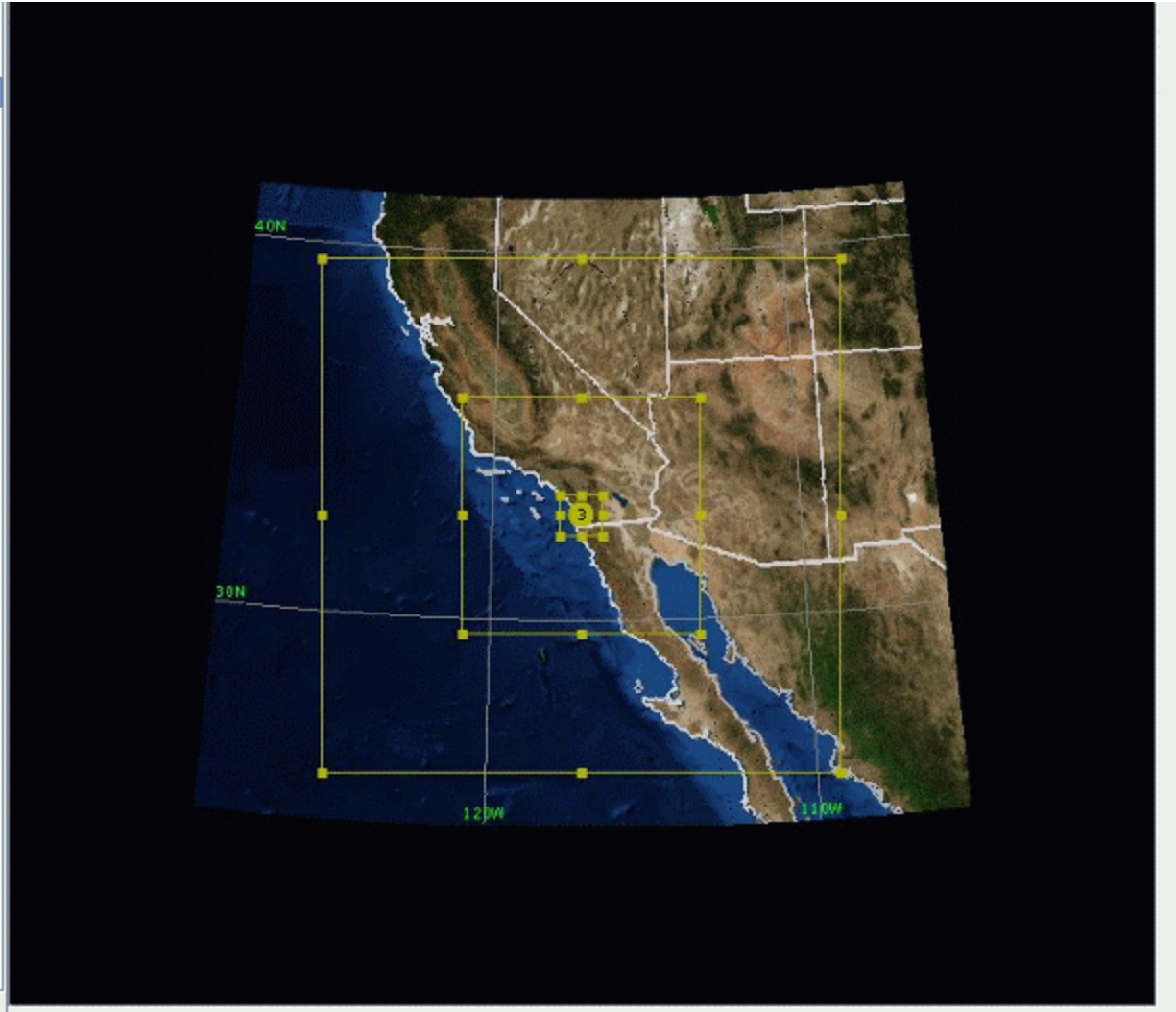


Figure 1. Domains 1, 2, 3 (9, 3, and 1-km grid spacing) centered over southern California for this experiment.

The National Centers for Environmental Prediction (NCEP) Global Forecast System (GFS)  $0.5^\circ$  horizontal grid-spacing output was used to create initial conditions and boundary conditions for the WRF. A higher-resolution product from NCEP called the Real Time Global Sea Surface Temperature has  $1/12^\circ$  horizontal grid spacing and was used to specify sea surface temperatures (7). Where available, GFS snow fields were replaced with 1-km snow fields from the National Weather Service's National Operational Hydrologic Remote Sensing Center Snow Data Assimilation System (8).

The Mellor-Yamada-Janjić (MYJ) scheme (9) was used to parameterize the atmospheric boundary layer. As in Lee et al. (10), the background turbulent kinetic energy (TKE) is decreased to better simulate conditions with low TKE and the above boundary layer depth diagnosis is altered. In preliminary experiments for this study, the standard MYJ scheme resulted in noisy TKE fields and thus noisy Planetary Boundary Layer (PBL) depth fields over the water. These were resolved using this altered version of MYJ. The other WRF parameterizations utilized

included Thompson's microphysics parameterization, the Kain-Fritsch cumulus parameterization, the Rapid Radiative Transfer Model for longwave radiation and the Dudhia scheme for shortwave radiation. The Noah land surface model is used to represent land surface processes (11).

---

## 4. Turbulence Evaluation

---

### 4.1 Techniques to Solve Turbulence

Turbulence can be generated by buoyant thermals and by mechanical eddies but it is suppressed by statically stable lapse rates and dissipated into heat by the effects of molecular viscosity. Physically, the TKE is characterized by measured root-mean-square velocity fluctuations. In Reynolds-averaged Navier Stokes equations, the TKE can be calculated based on the closure method, i.e., a turbulence model. Generally, the TKE can be quantified by the mean of the turbulence normal stresses as shown in equation 1, where  $\bar{e}$  represents an instantaneous TKE per unit mass (12).

$$\bar{e} = \frac{1}{2} \left( \overline{u'^2} + \overline{v'^2} + \overline{w'^2} \right) \quad (1)$$

Numerous scientists have attempted to use both theoretical and observational data to formulate techniques to forecast CAT. Dutton and Panofsky (13) associated vertical shear instabilities with turbulence. Bacmeister et al. (14) noted an obvious correlation between mountain waves and turbulence. Keller (15) developed the Specific CAT Risk index that relates the nonturbulent component of the tendency of the Richardson number to stretching deformation and shearing deformation. McCann (16) showed that correlation coefficients are rarely greater than  $\pm 0.35$  when using the existing methods. These are just a small sample of studies conducted to forecast or predict CAT, although, there will be a more detailed discussion on this topic later in the report.

### 4.2 ARL Turbulence

As previously noted, theoretical studies and empirical evidence have associated turbulence with instabilities. Miles and Howard (17) indicate that the development of these instabilities require the existence of a critical Richardson number (RI)  $\leq 0.25$ . Stull (18) notes that the Richardson number is a simplified term or approximation of the TKE equation where the RI is expressed as a ratio of the buoyancy resistance to energy available from the vertical shear.

The equation for the RI is expressed in equation 2:

$$RI = \frac{\frac{g}{\theta} * (\frac{\partial \theta}{\partial Z})}{(\frac{\partial V}{\partial Z})^2} \quad (2)$$

where  $g$  is the gravitational acceleration,  $\frac{\partial \theta}{\partial Z}$  is the change of potential temperature with height, and  $\partial V$  is the vector wind shear occurring over the vertical distance  $\partial Z$ .

Boyle (19) of The U.S. Navy Fleet Numerical Meteorological and Oceanography Center (FNMOC) used the Panofsky index (PI) to forecast low-level turbulence, where the low level is considered to be below 1220-m above ground level (AGL). The formula for this index is:

$$PI = (\text{windspeed})^2 * (1.0 - RI/RI_{\text{crit}}) \quad (3)$$

where RI is the Richardson number and  $RI_{\text{crit}}$  is a critical Richardson number empirically found to be 10.0 for the FNMOC data. The higher the PI the greater the intensity of turbulence at low levels.

Ellrod and Knapp (20) listed environments where significant CAT was found to be prevalent. Their study associated vertical wind shear (VWS), deformation (DEF), and convergence (CVG) into a single index as shown in equation 4, which is called the Turbulence index (TI).

$$TI = VWS * [DEF + CVG] \quad (4)$$

The deformation term is a combination of stretching deformation and shearing deformation.

Originally, of all the methods used to forecast turbulence using a single sounding, the RI seemed to make the most sense physically, since it included the influence of both the temperature and shear in the atmosphere. Based on the work of McCann (16), the RI also displayed the most skill of several methods tested. However, Passner (21) found in his study between 1995 and 1997 that the PI provided more skill than the RI in the lowest 1220 m AGL using upper-air observation data alone. Additionally, results showed that the RI was generally ineffective between 1524- to 3049-m AGL and although it was more effective above 3049-m AGL it underforecasted turbulence at all levels. Knapp et al. (22) used Higher Order Turbulence Model for Atmospheric Circulations (HOTMAC) mesoscale model output in their study. HOTMAC was a very coarse model with only 22 vertical levels and 20-km grid spacing at that time, although the model grid spacing was reduced to 10 km at a later date. Knapp noted that the TI was based on the frotogenesis equation and the results of his work indicated that DEF+CVG correlated best in the low levels implying that horizontal wind flow changes were more vital than vertical motion fields in determining turbulence in the low levels. Based on these results, Passner decided to combine the PI and TI for use in mesoscale model output and used the PI below 1220-m AGL and the TI above 1220-m AGL as the way to calculate turbulence from model output.

Each model grid point below 1220-m AGL was assigned a value of PI and each model point above 1220 m was assigned a value of TI. They were then classified to have “no” (NONE) turbulence, “light” (LGT) turbulence, “moderate” (MOD) turbulence, or “severe” (SEV) turbulence, which included severe or extreme forecasts of turbulence.

Further research by Passner (23), compared turbulence forecasts using both the 2-km WRF and the 18-km WRF over the northeastern U.S. in 2006 with 43 vertical sigma levels. Results showed that the low-level forecasts using PI were not influenced significantly by increasing the horizontal resolution. The turbulence YES/NO forecast bias for the 18-km WRF was 1.02 while the bias for the 2-km WRF was 1.19. However, there was a significant difference for turbulence above 1220-m AGL using the TI. The False Alarm Rate (FAR) for the YES/NO turbulence forecast increased, which lead to a bias of 1.31 at 18 km and a bias of 1.56 at 2 km. In general, these data for the entire experiment from August 2006 to April 2007 did show more intense and higher turbulence coverage at 2 km than at 18 km. For example, on the 18-km domain 40% of the forecasts were for MOD or SEV turbulence while 43% of the observations on those days were for MOD or SEV turbulence. On the 2-km domain, 58% of the forecasts were for MOD or SEV turbulence while 40% of the observations contained reports of MOD or SEV turbulence. Overall, using the 2-km output, 25 turbulence forecasts were for SEV turbulence but only four cases verified as SEV in the sample of 67 cases.

Meanwhile, a second test using unmanned aircraft systems (UAS) at Yuma Proving Ground, AZ, in 2007 showed an additional issue. To resolve the majority of the local terrain features of mesoscale meteorological significance, ARL attempted to resolve the lower levels by using more sigma levels in the lowest 305-m AGL and a total of 60 vertical levels (24).

There was a trend for areas of MOD or SEV turbulence in small areas each afternoon, although wind speeds and wind shear did not appear to increase significantly. After researching the problem, it became obvious that the height differences between the sigma levels were exceptionally small in the boundary and this led to significantly higher values of PI. The denominator in equation 2 became excessively large in the lowest four or five sigma levels due to the small values of  $\Delta Z$  (change of height). This led to values of PI of over 1,000 in some cases when even values of 250 are often related to SEV turbulence.

Thus, it was necessary to make the following adjustments as the ARL transitioned to higher-resolution WRF models in both the horizontal and vertical. The TI was adjusted to be parameterized based on the grid resolution. Cases were divided into two groups: one when the horizontal grid spacing was less than 8 km and one where it was greater than 8 km, thus, treating the turbulence forecasts as a parameterized product based on the horizontal scale. For smaller grid sizes, less than 8 km, the categories for LGT, MOD, and SEV turbulence were adjusted to remove the bias of MOD and SEV turbulence (table 1). Finally, some “sanity” checks were

added to the software to look for excessive turbulence forecasts, especially in the area of 1220- to 2439-m AGL. In addition, changes were made in the layers above 2439-m AGL to remove biases.

Table 1. Criteria for turbulence intensity used by ARL.

	<b>NONE</b>	<b>LGT</b>	<b>MOD</b>	<b>SEV</b>
PI	<50.0	50–150	150–500	500+
TI (delta x<8)	<10.0	10–20	20–50	>50.0
TI (delta x>=8)	<3.0	3–9	9–18	>18.0

### 4.3 AFWA Turbulence

Similar to the work at ARL, AFWA’s turbulence work by Brooks et al. (25) describe the turbulence forecasts and evaluation using the 45-km Mesoscale Model Version 5. AFWA tried many different experiments using PI for low-level turbulence and TI for higher levels. Results were similar to the work done at ARL at the same time. Currently AFWA is using the PI to 1524-m AGL with only minor differences in the calculation of the PI and the same calculations used to find TI above 1524-m AGL. AFWA does not use the “checks” that ARL applies to see if no turbulence is forecasted in high-wind cases or SEV turbulence is forecasted with light winds; however, it is uncertain if those “checks” are needed since no verification has been completed to test them. Additionally, AFWA does not attempt to parameterize or divide the turbulence forecasts based on horizontal grid resolution. In table 2 the values used to forecast turbulence and turbulence intensity are shown.

Table 2. Criteria for turbulence and intensity used by AFWA.

	<b>NONE</b>	<b>LGT</b>	<b>MOD</b>	<b>SEV</b>
PI	<20.0	20–100	100–250	250+
TI	<3.0	3–9	9–14	>14.0

This AFWA algorithm has been developed using the 15-km WRF, although some areas of 5-km grid spacing are used for smaller domains. Because those 5-km domains are not available at all locations, the 15-km data was chosen so that products may be implemented for nearly every location of interest (26), but these same criteria are used for both the AFWA 5-m and 1.67-km grids.

McCormick (27), referring to AFWA’s algorithm, points out the PI does well in some cases, such as areas of strong winds or areas of intense low-level instability. However, the PI struggles in several other areas, such as cases where low-level instability does not reach a given threshold, or cases of turbulent waves.

### 4.4 McCann’s Boundary-Layer Turbulence (BLTURB) Method

McCann (28) used a theoretical approach to BLTURB. McCann notes that TKE equations are the basis for understanding turbulence in the PBL. The simplest form is a steady-state first order

equation in which turbulence is assumed to be analogous to diffusion. Equation 5 shows what is known as the flux-gradient TKE or K-closure equation because of the constants  $K_m$  and  $K_h$  where  $K_m$  is the eddy viscosity and  $K_h$  is the eddy thermal diffusivity.  $K_m$  is calculated as the difference between the current sigma level and the surface elevation multiplied by 0.054.  $K_h$  is the value of  $K_m$  multiplied by 4.0.

$$\varepsilon = K_m \left( \frac{\partial V}{\partial Z} \right)^2 - K_h \frac{g}{\theta_v} \frac{\partial \theta_v}{\partial Z} \quad (5)$$

The term on the left of equation 5 is the TKE dissipation due to molecular viscosity while the two terms on the right-hand side are the TKE production terms due to wind shear and stability. In this equation,  $\theta_v$  represents the mean virtual potential temperature and  $g$  is the acceleration due to gravity.

McCann's program takes model data output and computes BLTURB. The software works from the surface to the top of the boundary layer, which is a derived product from the WRF output files. McCann mentions that equations such as the RI can give an indication of turbulence but it does not give an indication of how strong the turbulence is. However, the TKE equation computes the amount of turbulence based on the quantity of positive TKE production. McCann, through experimentation, determined the correlation of the TKE output to turbulence intensity as see in table 3.

Table 3. Criteria for turbulence and intensity used by the BLTURB.

	<b>NONE</b>	<b>LGT</b>	<b>MOD</b>	<b>SEV</b>
BLTURB	<0.01	0.01–0.16	0.16–0.35	>0.35

#### 4.5. Unified Post Processor Turbulence

The NCEP Unified Post Processor (UPP) has replaced the WRF Post Processor (WPP). The UPP software package is based on WPP but has enhanced capabilities to postprocess output from a variety of Numerical Weather Prediction (NWP) models, including WRF-ARW, Nonhydrostatic Multiscale Model WRF-NMM, GFS, and Climate Forecast System.

UPP interpolates output from the model's native grids to National Weather Service (NWS) standard levels (pressure, height, etc.) and standard output grids (Advanced Weather Interactive Processing System, Lambert Conformal, polar-stereographic, etc.) in NWS and World Meteorological Organization Gridded Binary format. There is also an option to output fields on the model's native vertical levels. UPP outputs hundreds of possible fields such as temperature, height, humidity, cloud water, rain, snow, wind fields, and aviation products. Included in the aviation products are wind shear, ceiling, icing, and CAT. The UPPV1.0 and UPPV2.0 software

use the TI index from the surface to the model top (29). Table 4 shows the values to define turbulence and turbulence intensity.

Table 4. Criteria for turbulence and intensity used by the UPP.

	<b>None</b>	<b>LGT</b>	<b>MOD</b>	<b>SEV</b>
TI	<4.0	4–8	8–12	>12.0

#### 4.6 Explicit TKE Predicted by the WRF

The BLTURB mixing was parameterized in the WRF-ARW using the MYJ PBL scheme (9), which is a 2.5 level closure model. The equation to express TKE is expressed in equation 6.

$$\frac{d\left(\frac{q^2}{2}\right)}{dt} - \frac{\partial}{\partial z} \left[ l_m q S_q \frac{\partial}{\partial z} \left( \frac{q^2}{2} \right) \right] = P_s + P_b + \varepsilon \quad (6)$$

Where the first term on the left-hand side represents the total derivative of  $q=(2 \times \text{TKE})$  and the second term is the vertical redistribution of  $q$ . The terms on the right-hand side of equation 6 represents the production of  $q$  by shear and buoyancy, respectively, while the last term is the dissipation (30).

The additional terms are:

$l_m$  = mixing length

$s_q$  = determined from experimental data.

The values of explicit model-derived TKE are determined by the MYJ scheme can be displayed in WRF-ARW by using the Grid Analysis and Display System.

---

## 5. Turbulence Evaluation

---

The method used in this study to verify turbulence is to compare PIREPs to model forecasts. Using the WRF output, verification is limited to a 1-h period surrounding the model forecast time. As an example, model forecasts of turbulence at 2100 UTC are compared to PIREPs from 2030 to 2130 UTC only. Any PIREPs that included two intensities, such as LGT to MOD, were classified as the more extreme intensity, MOD in this case. As a standard, only PIREPs close in height to the model forecast were accepted. For levels below 3049-m AGL, the forecasted turbulence had to be within 305 ft of the PIREP. From 3049- to 6098-m AGL, the forecast had to be within 457 m of the PIREP, and above 6098-m AGL, the forecast had to be within 610 m of the observed turbulence.

The turbulence evaluation, while very limited, was done on five days: 16 February 2012, 1 March 2012, 5 March 2012 over the Los Angeles International Airport (LAX) area, 2 May 2013 over the Dallas/Fort Worth International Airport (DFW) grid, and 13 May 2013 over the New Jersey and New York metropolitan area. These days were selected based on terrain and diverse weather conditions. The LAX grids were evaluated over the 3-km domain in an effort to get more PIREPS than those on the smaller 1-km domain. The two cases in May were evaluated using the AFWA 1.67-km grids.

The results for “YES/NO” turbulence forecasts are shown in table 5 for each method tested where POD is Probability of Detection, FAR is False Alarm Ratio, TSS is True Skill Score, and Bias is the bias to overforecast or underforecast an event. A value of over 1.0 is considered an “overforecast” while a value under 1.0 is an “underforecast” bias.

Table 5. “YES/NO” turbulence forecasts for the five days studied.

	<b>POD</b>	<b>FAR</b>	<b>TSS</b>	<b>Bias</b>
ARL	0.74	0.10	0.18	0.82
AFWA	0.83	0.09	0.27	0.91
UPP	0.88	0.09	0.32	0.96
BLTURB	0.25	0.00	-0.75	0.25

The results in table 5 should be used with caution since they are based on 66 PIREPs, of which about half of the sample occurred on a major turbulence day over the LAX area (16 February 2012). As can be seen, the POD is exceptional for the sample using the ARL, AFWA, and UPP method while the FAR is low. The forecasts predict turbulence less than 6098-m AGL only. The BLTURB routine only had 17 samples since the routine is designed to only work to the top of the boundary layer determined by the WRF. It managed to only correctly forecast CAT in four of the 17 cases that were observed in the boundary layer. Verifying low-level turbulence becomes excessively difficult since there are so few PIREPs near the surface and the PBL often is very low near the Pacific Ocean in the cold season in California. It is uncertain if the verification of the BLTURB has any value in this study, but certain trends can be found in these data.

Turbulence intensity was another focus area in this study. The different turbulent forecasting methods did provide a wide range of results. Table 6 shows the forecasted and observed turbulence intensities based on the 66 PIREPs.

Table 6. Turbulence intensities from the ARL routine. The number of forecasts in each group is the vertical total and the number of observations in each group is the horizontal total.

	<b>NONE</b>	<b>LGT</b>	<b>MOD</b>	<b>SEV</b>	<b>Total</b>
NONE	5	3	1	1	<b>10</b>
LGT	4	3	2	2	<b>11</b>
MOD	10	10	12	6	<b>38</b>
SEV	0	0	4	3	<b>7</b>
<b>Total</b>	<b>19</b>	<b>16</b>	<b>19</b>	<b>12</b>	<b>66</b>

In table 6, as an example, there are 38 cases of MOD turbulence observed while there are 19 forecasts of MOD turbulence. Table 7 shows the AFWA forecast intensity, table 8 displays the UPP intensity forecasts, and table 9 the BLTURB intensities.

Table 7. Turbulence intensities from the UPP routine. For each group the number of forecasts is the vertical total and the number of observations is the horizontal total.

	<b>NONE</b>	<b>LGT</b>	<b>MOD</b>	<b>SEV</b>	<b>Total</b>
NONE	4	1	2	3	<b>10</b>
LGT	4	1	0	6	<b>11</b>
MOD	4	2	3	29	<b>38</b>
SEV	0	0	0	7	<b>7</b>
<b>Total</b>	<b>12</b>	<b>4</b>	<b>5</b>	<b>45</b>	<b>66</b>

Table 8. Turbulence intensities from the AFWA routine. For each group the number of forecasts is the vertical total and the number of observations is the horizontal total.

	<b>NONE</b>	<b>LGT</b>	<b>MOD</b>	<b>SEV</b>	<b>Total</b>
NONE	5	3	1	1	<b>10</b>
LGT	2	1	2	6	<b>11</b>
MOD	8	2	7	21	<b>38</b>
SEV	0	0	1	6	<b>7</b>
<b>Total</b>	<b>15</b>	<b>4</b>	<b>11</b>	<b>36</b>	<b>66</b>

Table 9. Turbulence intensities from the BLTURB routine. For each group the number of forecasts is the vertical total and the number of observations is the horizontal total.

	<b>NONE</b>	<b>LGT</b>	<b>MOD</b>	<b>SEV</b>	<b>Total</b>
NONE	0	0	0	0	<b>0</b>
LGT	2	0	0	0	<b>2</b>
MOD	9	3	0	0	<b>12</b>
SEV	2	1	0	0	<b>3</b>
<b>Total</b>	<b>13</b>	<b>4</b>	<b>0</b>	<b>0</b>	<b>17</b>

The results show that the ARL routine tends to underforecast the MOD turbulence events slightly, but the AFWA and UPP have a strong bias to overforecast the turbulence intensity as SEV as the UPP forecasted SEV in 68% of the forecast, while the ARL routine only forecasts SEV turbulence in 18% of the sample. In this study, 10% of all the PIREPs were SEV, which is a higher number than might be expected. However, that bias can be explained by the strong, dynamic weather event and turbulence event on 16 February 2013 over the LAX area. The case study from the DFW area on 2 May 2013 was chosen because of the strong northerly flow behind a departing weather system that day in the southern plains. Winds by late afternoon were 18 m/s (not shown) at 700-m AGL. The ARL, AFWA, and UPP routines all handled the turbulence forecasts well in that case.

However, on 13 May 2013 over the New Jersey/New York area the forecasts missed a case with several pilots reporting MOD turbulence below 1220-m AGL. Several observation stations in New Jersey were reporting gusty surface conditions with broken clouds that may have contributed to the turbulence. However, the ARL, AFWA, BLTURB, and UPP routines did not forecast turbulence. It is possible that the predictions missed what appears to be a moderately unstable low-level lapse rate.

Evaluation of the model-derived TKE (from equation 6) was more problematic since there are no known studies to relate values of WRF TKE values to observed CAT. However, in this study, it was found that in all 20 cases where TKE was greater than 0.50, turbulence was reported. While this is a small sample, perhaps it is an excellent starting point to use TKE as a predictor for turbulence below 1524-m AGL. When TKE was less than or equal to 0.50, turbulence was reported in only 16% of the cases below 1524-m AGL. Most of the calculations of TKE above 1524-m AGL were recorded as 0.009, or approximately 0.

A comparison of the five methods for a single case provided a useful “eye ball” evaluation that matched the trends of the statistical evaluation. The 16 February 2012 case was an ideal day to examine, since it was a day with numerous turbulence reports from pilots in the area with many reporting MOD or SEV turbulence.

The 1500 UTC upper-air observation at Edwards Air Force Base is shown in figure 2, while the 500-hPa upper-air map is displayed in figure 3. The sounding indicates a layer of strong winds just above the surface from a northeast direction—a down slope component off the higher terrain to the east. The upper low, at 1200 UTC, is on the south part of the grid, with the 500-hPa winds from the northeast. The air mass is unseasonably cold aloft with temperatures near  $-10^{\circ}\text{C}$  at 700 hPa and  $-27^{\circ}\text{C}$  at 500 hPa. The 1200 UTC upper-air observation at San Diego, CA (not shown), showed strong directional shear near the surface with northwest winds along the coast and a northeast wind about 305-m AGL. This indicated shearing winds near the ground, which can contribute to turbulence.

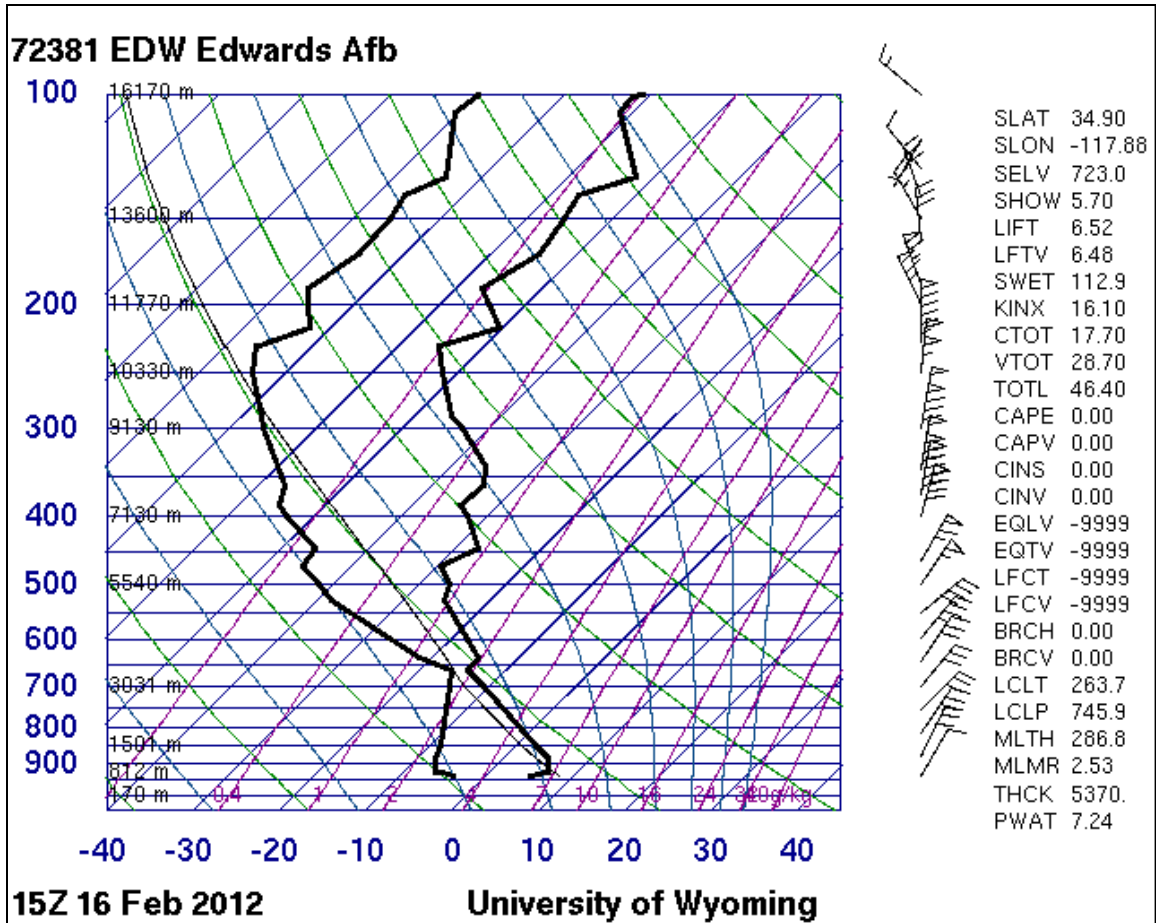
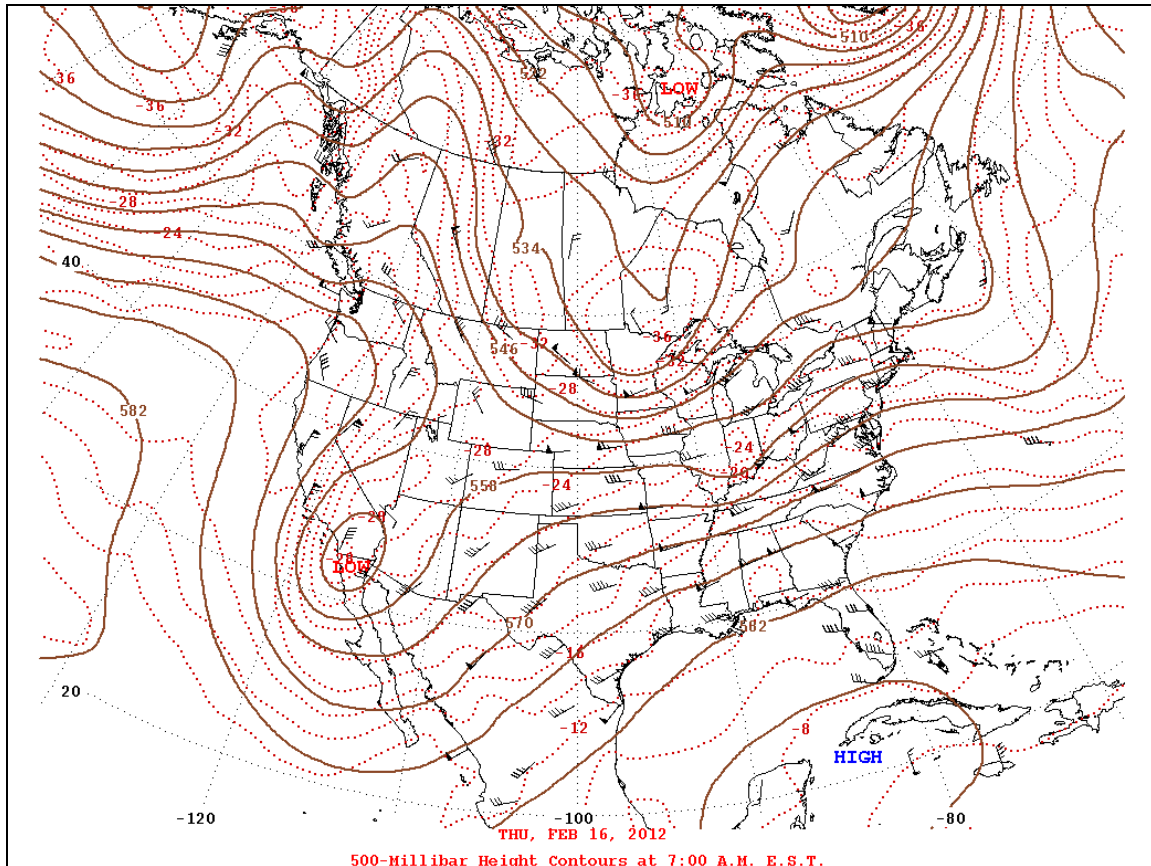


Figure 2. The upper-air observation from Edwards Air Force Base at 1500 UTC on 16 February 2012.

Note: Figure 2 is provided courtesy of the University of Wyoming, Department of Atmospheric Sciences (31).



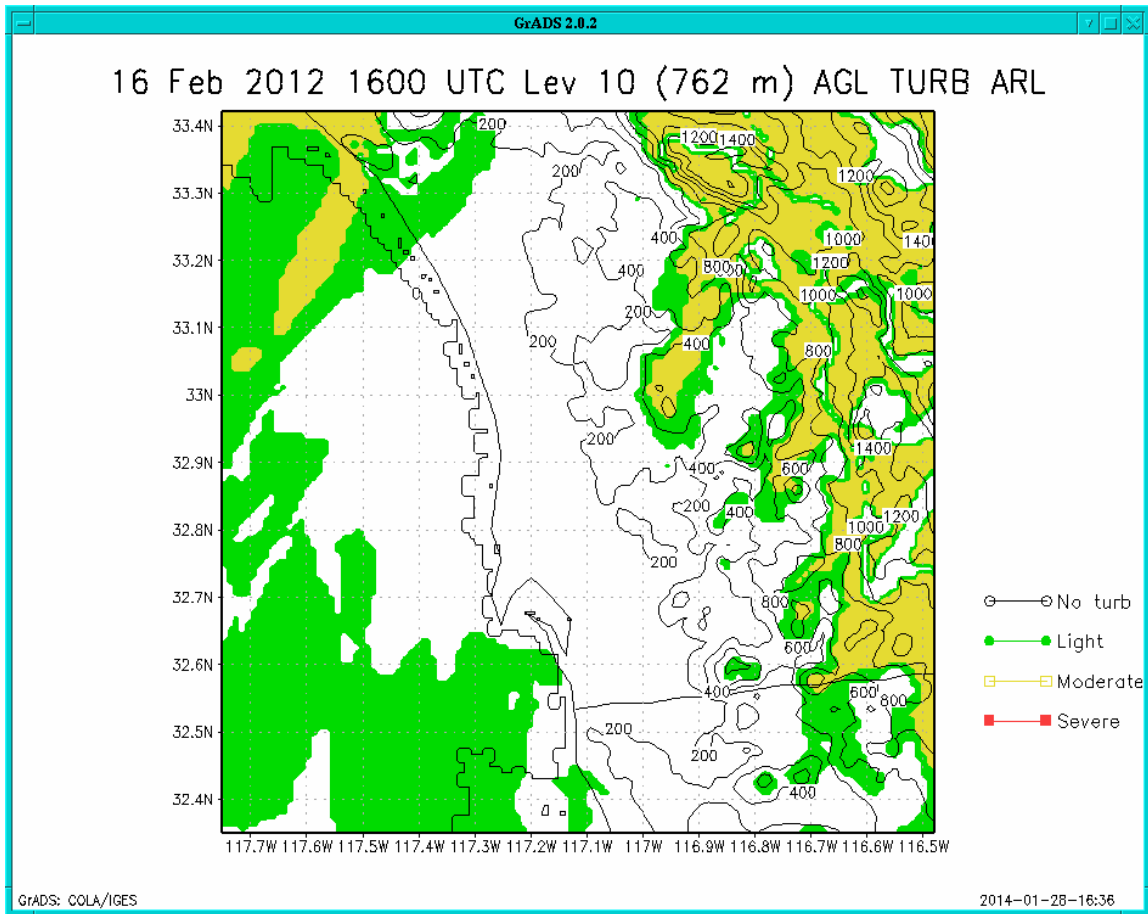


Figure 4. ARL turbulence forecast method at 1600 UTC for level 10 on 16 February 2012.

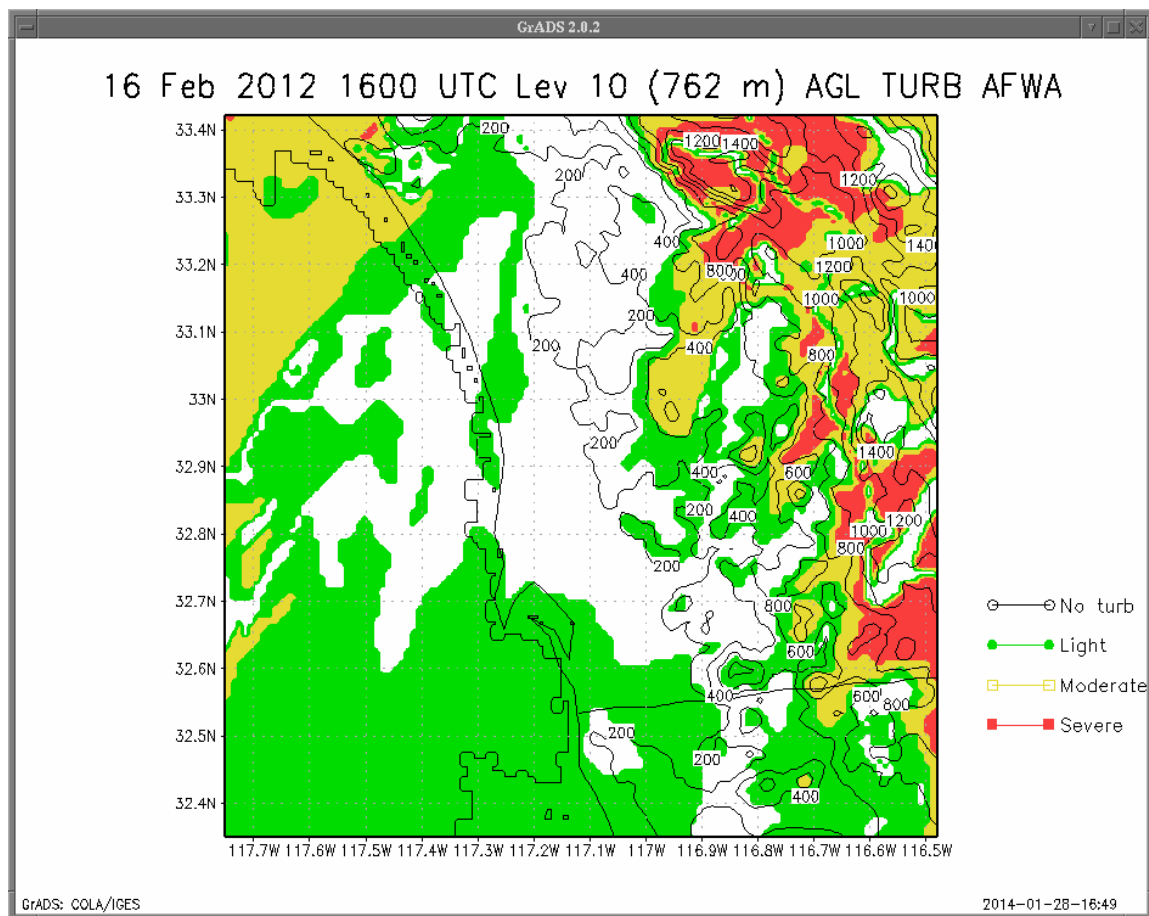


Figure 5. AFWA turbulence forecast method at 1600 UTC for level 10 on 16 February 2012.

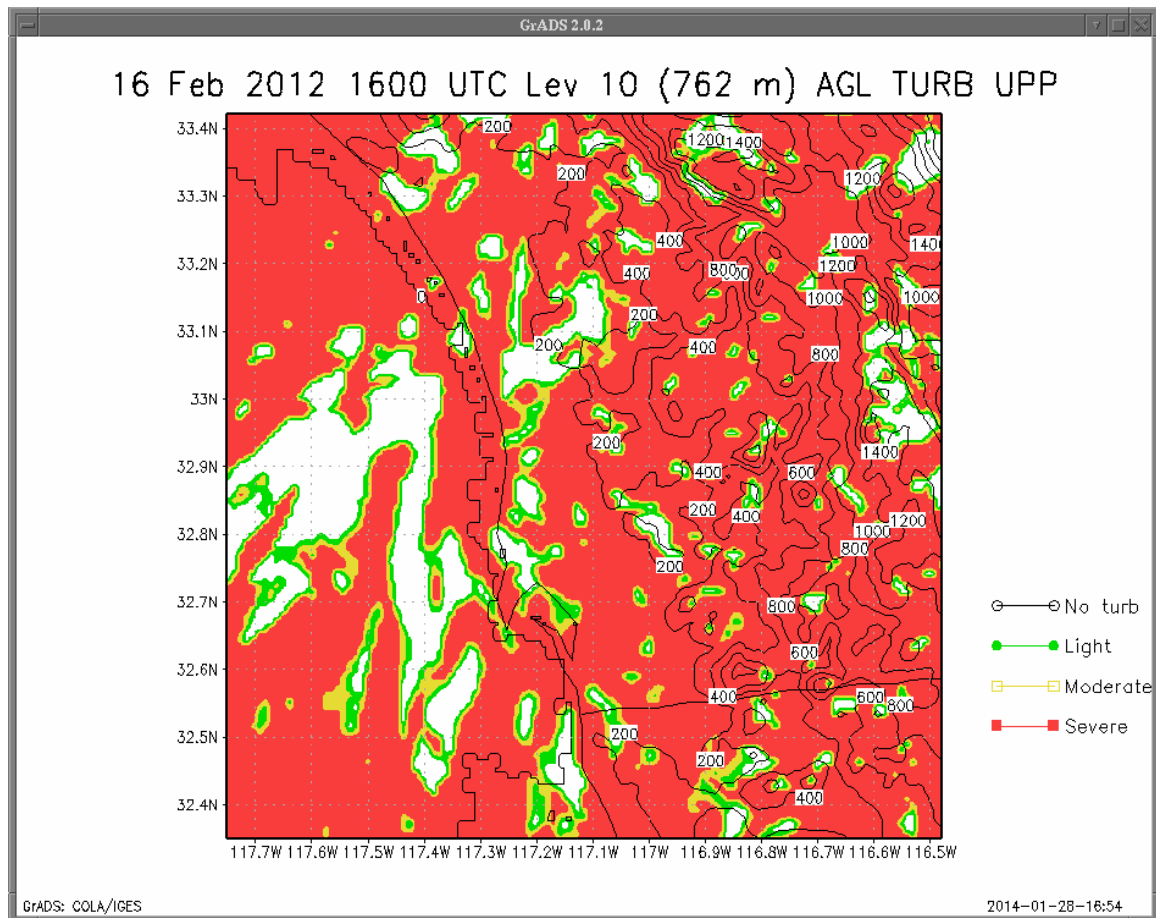


Figure 6. UPP turbulence forecast method at 1600 UTC for level 10 on 16 February 2012.

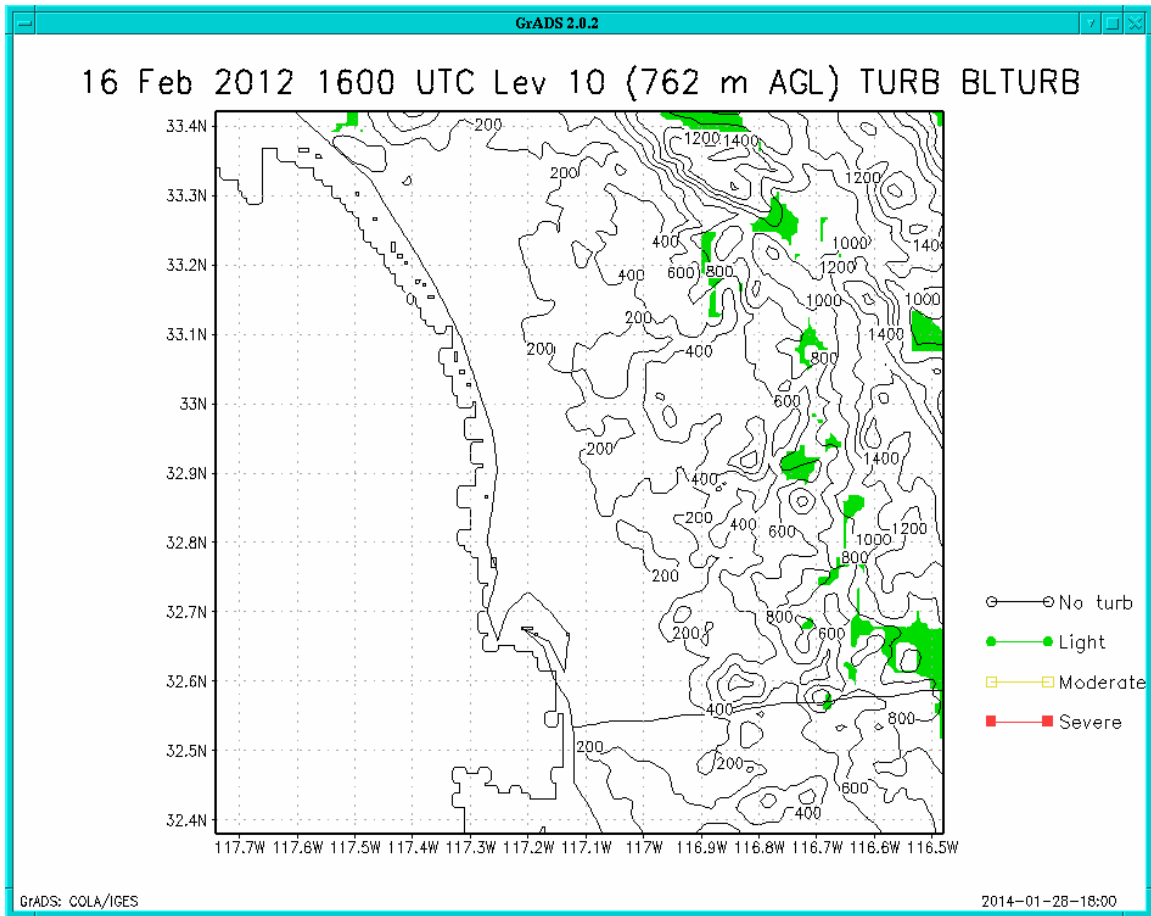


Figure 7. BLTURB forecast method for turbulence at 1600 UTC at level 10 on 16 February 2012.

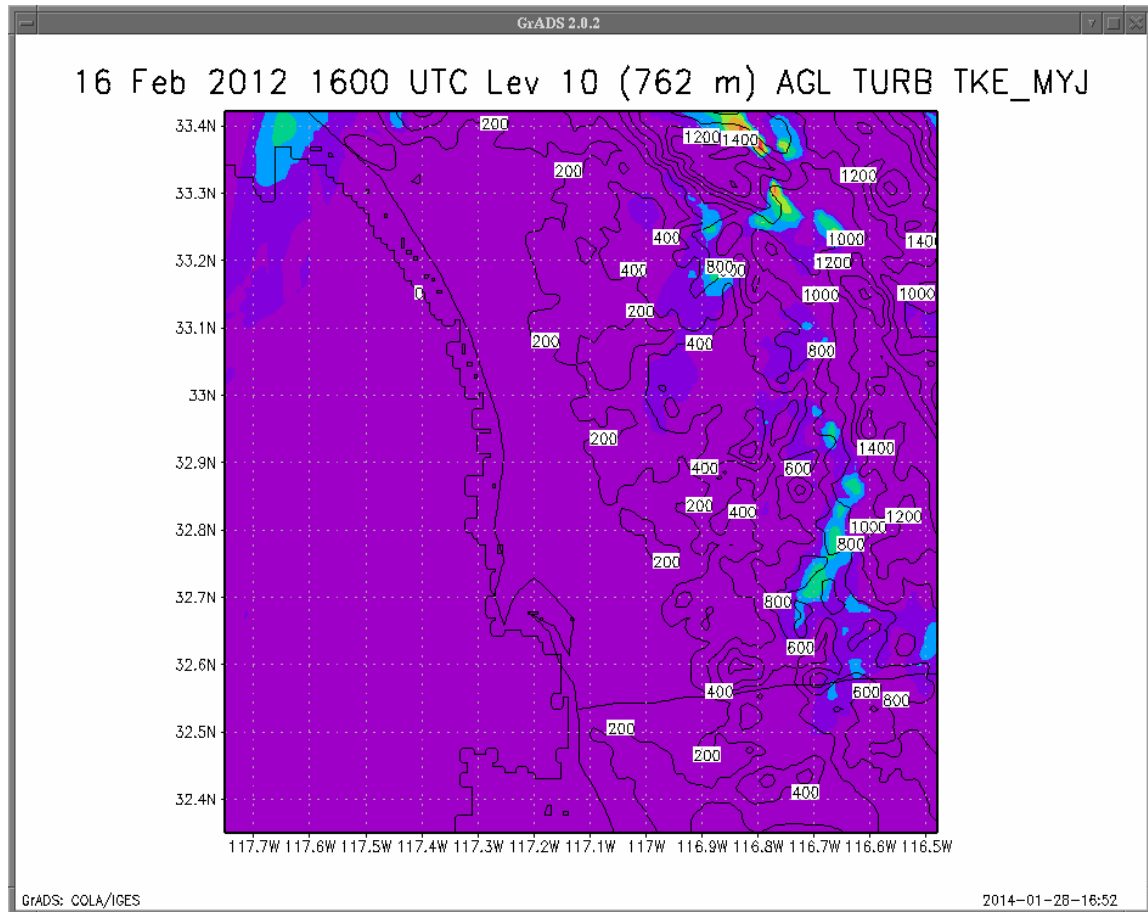


Figure 8. MYJ PBL TKE forecast method for turbulence at 1600 UTC on level 10 on 16 February 2012.

### 5.1 Case of 13 May 2013 in the Northeast USA—Instability and Turbulence

In this case, the horizontal and vertical spacing was different than the cases examined over southern California. The number of sigma levels was increased in the lowest 1524-m AGL, and decreased in the middle levels of the atmosphere. Another change was to use two nests as suggested by AFWA, with the outer nest having a 5-km grid spacing and the inner nest a 1.67-km grid spacing. Domain 1 was  $200 \times 200$  grid points, while domain 2 was  $202 \times 202$  grid points. The model ran with 57 vertical levels. As part of this experiment, the model physics and model dynamics were nearly identical to those used by AFWA. While ARL ran a similar configuration to AFWA, these results are not directly from an AFWA operational run, and there will be some differences.

The day started with a deep, cold 500-hPa upper-low centered over southeast Canada with a trof axis trailing through New York, Pennsylvania, West Virginia, and southward as seen in figure 10. The region was under a strong westerly flow aloft as seen on the 1200 UTC, Upton, NY sounding in figure 9; however, winds at the surface and just above were not as strong. At 1600 UTC, surface winds of 5 to 8 m/s were observed with occasional gusts to 10 m/s. At 1400

UTC, surface observers were indicating a broken deck of clouds between 1677- and 1829-m AGL. The 1645 UTC satellite (figure 11) indicates a large area of cloud cover over the entire region. Meanwhile, many pilots were reporting MOD turbulence from 762- to 1220-m mean sea level (MSL) between 1400 UTC and 2000 UTC, with most of these reports centered over New Jersey and southern New York State.

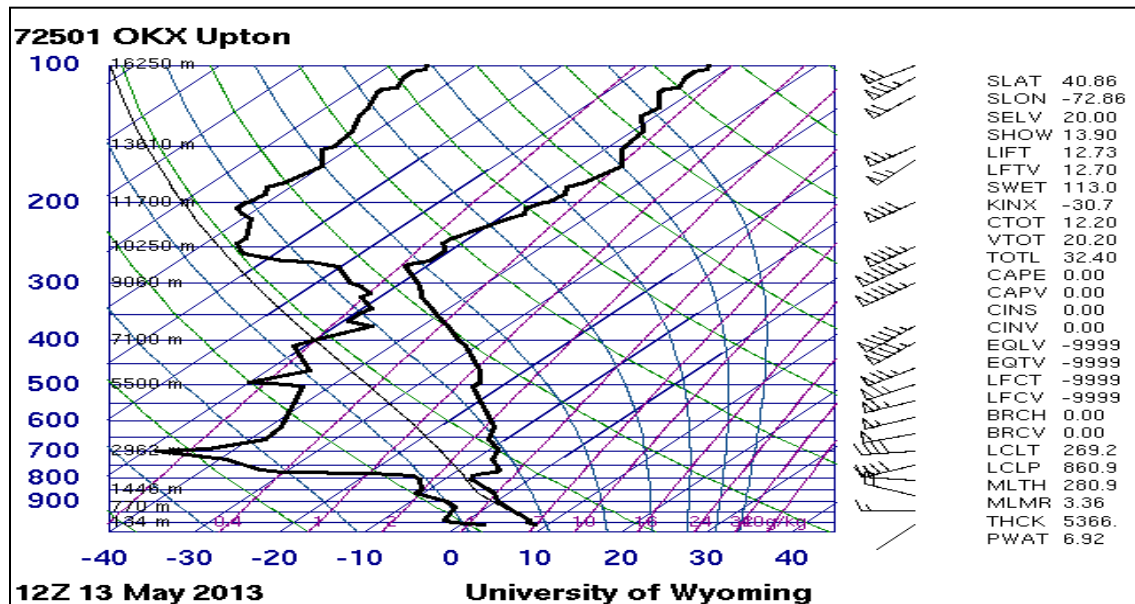


Figure 9. At 1200 UTC on 13 May 2013, upper-air observation at Upton, NY.

Note: Figure 9 is provided courtesy of the University of Wyoming, Department of Atmospheric Sciences (31).

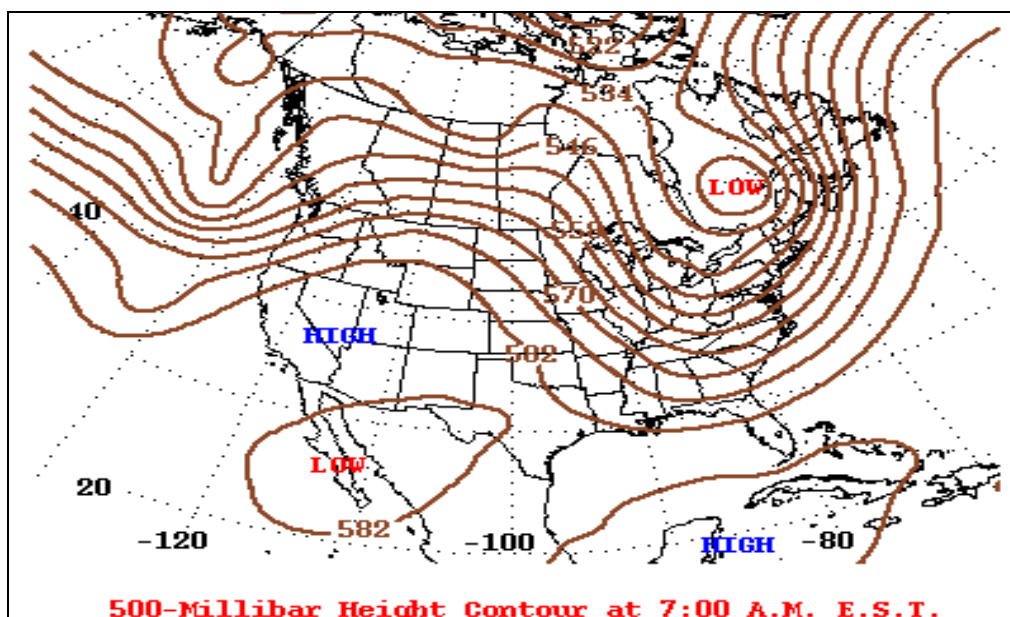


Figure 10. At 1200 UTC on 13 May 2013, 500-hPa heights.

Note: Figure 10 is provided courtesy of the NCEP Hydrometeorological Prediction Center (32).

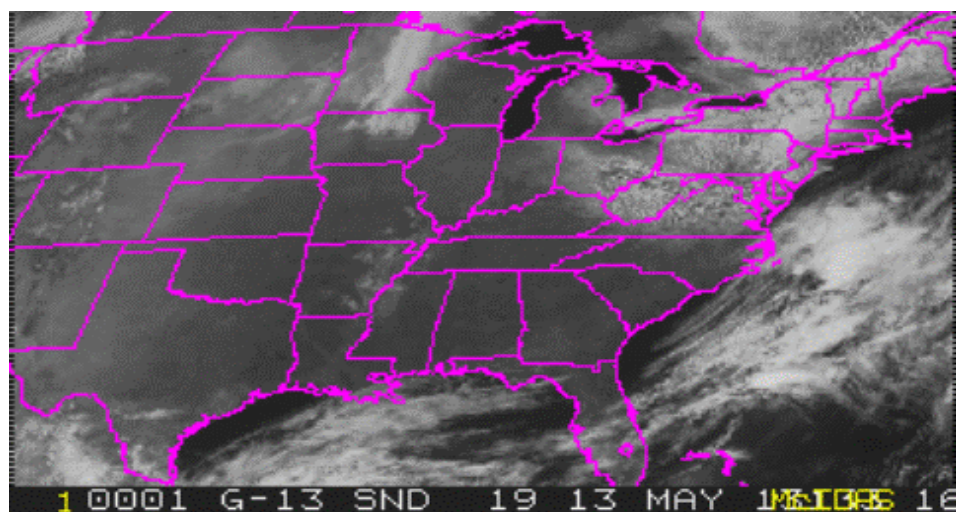


Figure 11. Satellite photo from 1645 UTC on 13 May 2013.

Note: Figure 11 is provided courtesy of Space Science and Engineering Center (SSEC), University of Wisconsin-Madison (33).

The ARL turbulence forecast at 1700 UTC is shown in figure 12. The plot shows a forecast for scattered areas of LGT turbulence at 915-m AGL, which is the average level that pilots were reporting MOD turbulence. This corresponds to sigma level 22 in the model output. The AFWA turbulence routine (not shown) provided a near replica of the ARL forecast since both are using the PI to calculate turbulence at this level.

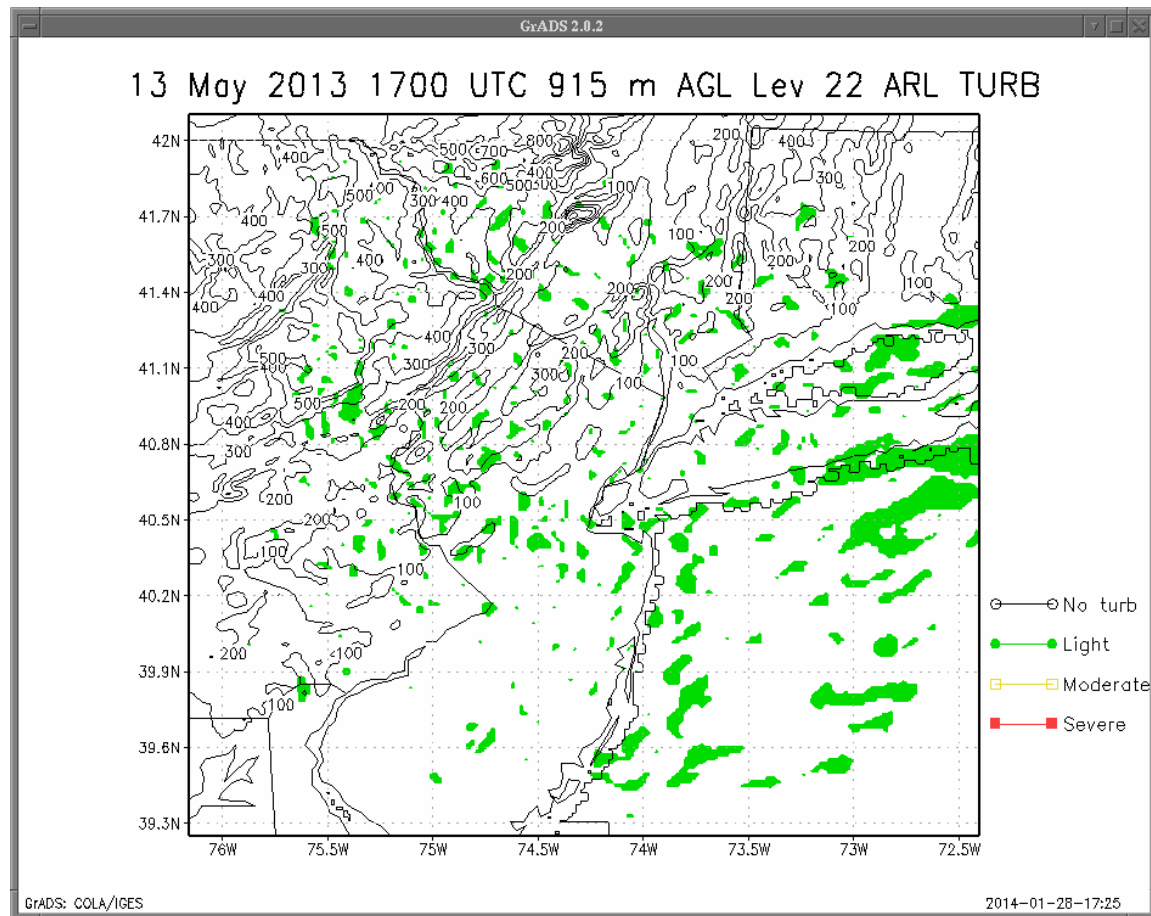


Figure 12. Turbulence forecast at 1700 UTC on 13 May 2013 using the ARL forecasting routine at level 22.

The WRF forecasted winds at 1700 UTC (figure 13) indicate wind speeds of 7 to 11 m/s over the area of interest at sigma level 22. These winds are not particularly strong, so using the PI it is likely that the RI term is causing the turbulence. To support this, on the 1200 UTC upper-air observation there is nearly a dry adiabatic lapse rate between 810 and 850 hPa with an inversion noted at about 778 hPa as shown in figure 9.

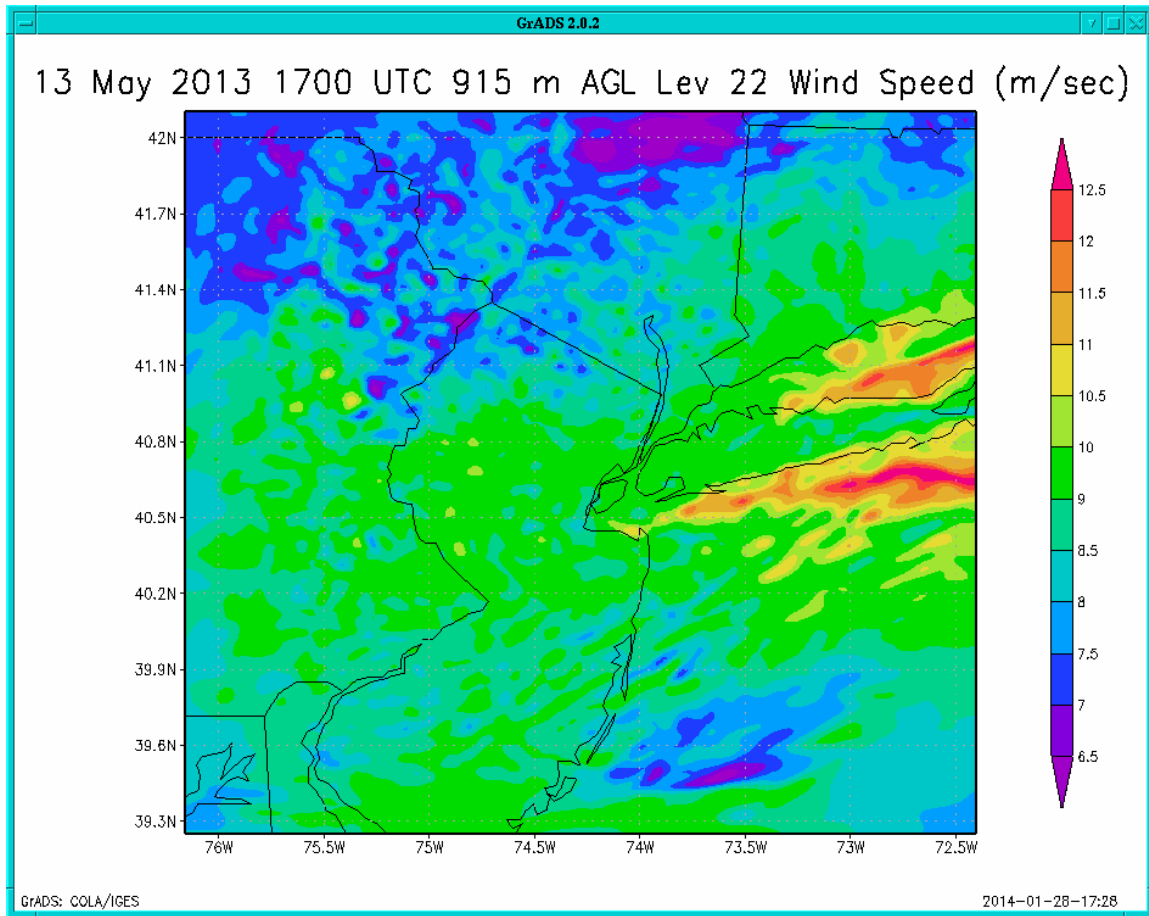


Figure 13. WRF forecasted wind speed at 915-m AGL at 1700 UTC on 13 May 2013 for level 22.

To explore this case, a random point at 40.8 N and 74.6 W was chosen to inspect the forecasted vertical profile of the atmosphere at that location. Starting with figure 14, the relative humidity is displayed with the values of qcloud (cloud water mixing ratio) and the  $w$  (m/s) wind component in figures 15 and 16, respectively. The relative humidity (RH) and qcloud plot show a sharp increase in moisture and model-derived qcloud in the sigma layers 25 to 30. In addition, the vertical motion profile shows rising motion in the same layer. This supports the idea that turbulence was possible in the layers at and below this moist and unstable layer. While there is little change of wind speed with height in the lowest 1524-m AGL (not shown), the steep lapse rate does lead to a higher RI, which would lead to a lower PI in the final calculation and a lower predictability of turbulence. This may explain why the forecast was for only areas of scattered LGT in the forecast.

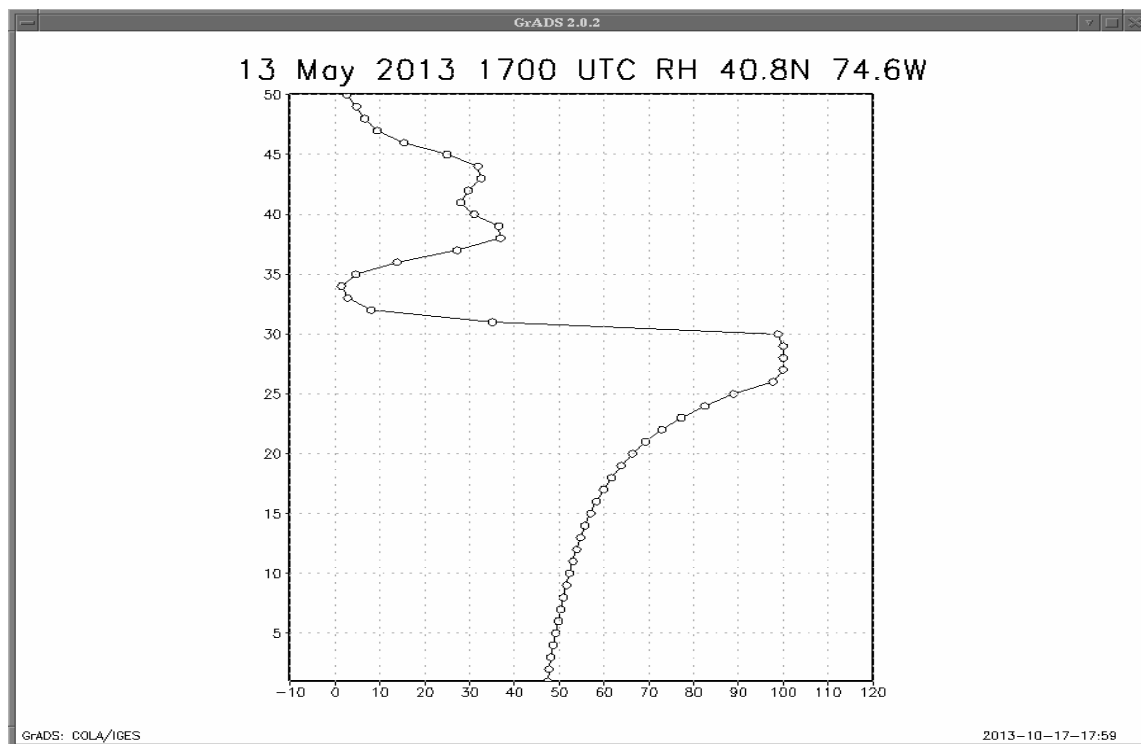


Figure 14. Vertical profile of RH (percent) forecasted for 1700 UTC at location 40.8° N 74.6° W on 13 May 2013.

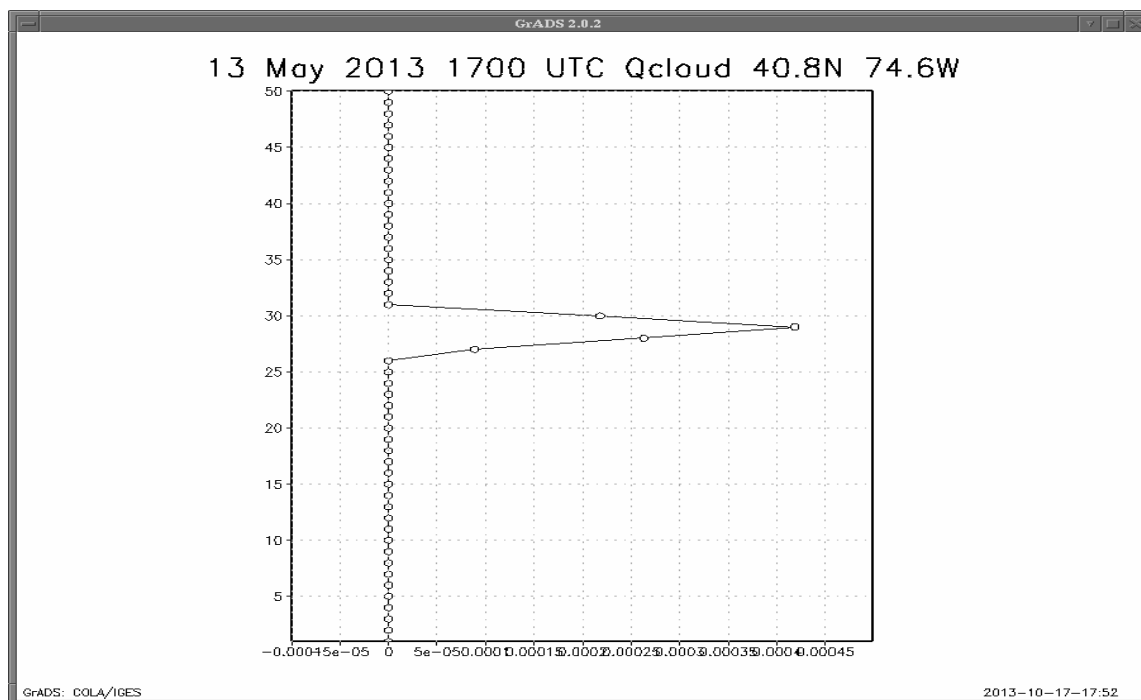


Figure 15. Vertical profile of qcloud (kg/kg) forecasted for 1700 UTC at location 40.8° N 74.6° W on 13 May 2013.

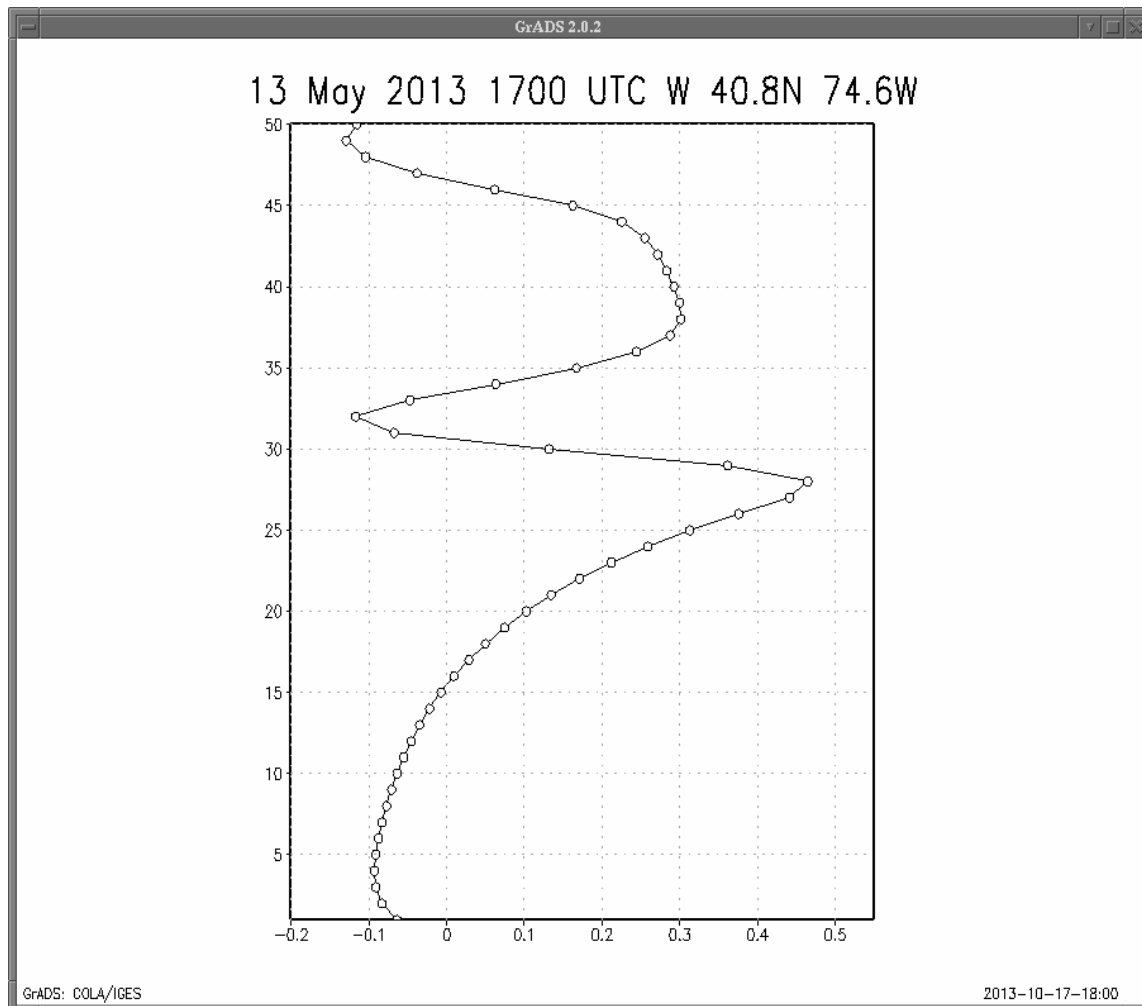


Figure 16. Vertical Profile of W (m/s) forecasted at 1700 UTC at location 40.8° N 74.6° W on 13 May 2013.

The vertical resolution of the model and available initial data may be inadequate to correctly find these small layers of instability; however, in this case the increased vertical resolution near the surface may have helped to find the moist and unstable layers.

Moisture fields are rarely considered as a source of turbulence, but lifting of moisture can create localized and small-scale turbulence due to subcloud processes, radiative heat exchanges, evaporation, or a number of other microscale processes. While much of this is speculation, and is difficult to verify, it becomes a future option to study the microphysical processes that may also have some influence on aircraft, especially smaller aircraft such as UAS. At the current time, much of the emphasis on the turbulence routines has been on buoyancy and wind shear. Additionally, almost all of the moisture incorporated in turbulence forecasting involves large-scale convection process, but smaller and shallow convection can contribute to turbulence as this case may indicate.

## 5.2 Convective Turbulence and Outflow

In addition to shallow convection, it is also interesting to look at more typical cases of deep convection often seen in the summer “monsoon” season in the desert southwest. Often these cases feature mid-level moisture and a very well-mixed boundary layer as seen in the sounding displayed in figure 17. This type of upper-air observation shows what is often called an “inverted V” sounding.

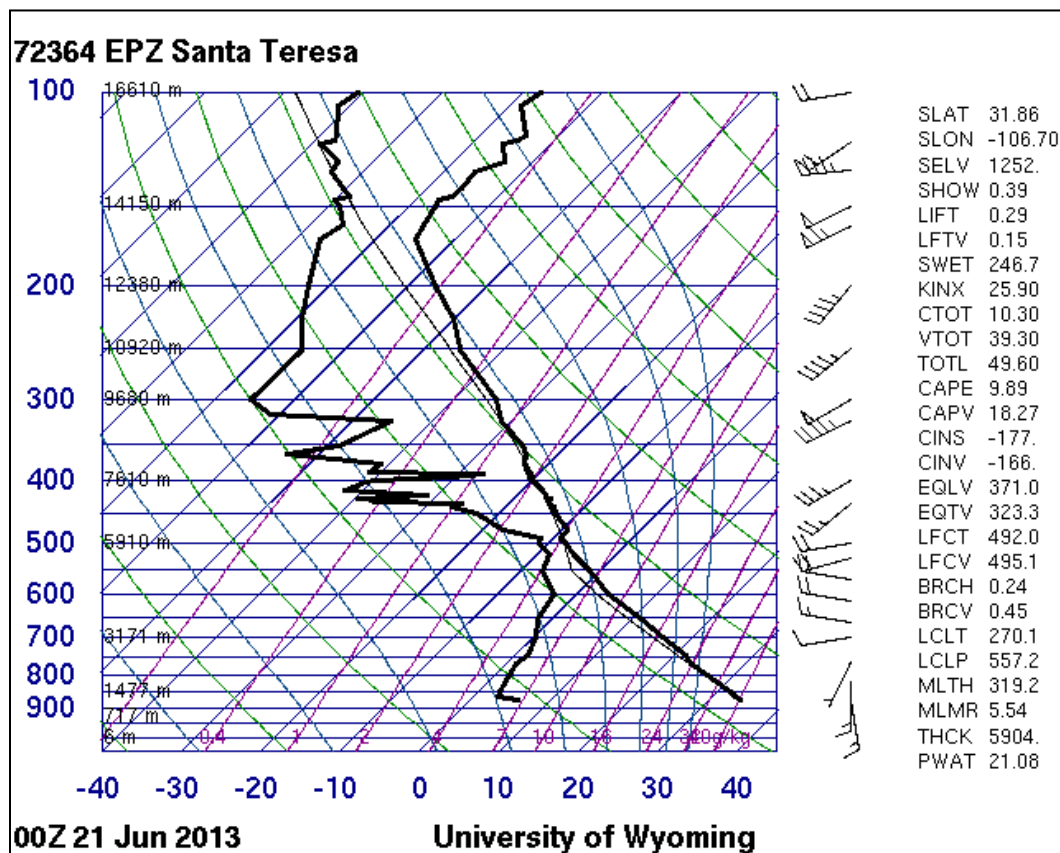


Figure 17. Upper-air observation at Santa Teresa, NM (EPZ) at 0000 UTC on 21 June 2013.

Note: Figure 17 is provided courtesy of the University of Wyoming, Department of Atmospheric Sciences (31).

Boundary-layer winds were from the southeast, but the wind direction may have been determined by local convection at the time of the sounding observation. The 1-km mosaic Next-Generation Radar (figure 18) at 2326 UTC does show convection in the region, with the heaviest rain to the south and southeast of El Paso, TX. A second line of lighter showers was noted from near the Las Cruces International Airport (LRU) southwestward into northern Mexico. It is uncertain if any of that precipitation was reaching the surface in the LRU area, thus setting up the environment for evaporation and strong downdrafts.

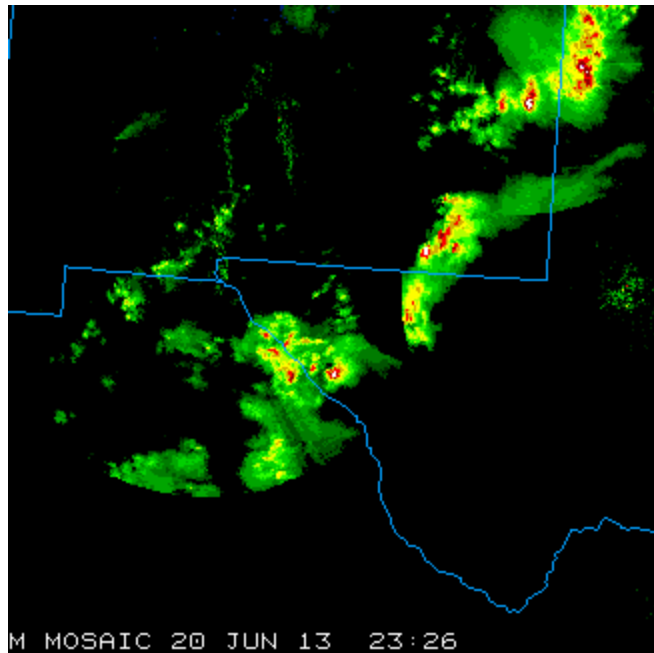


Figure 18. Radar image at 2326 UTC on 20 June 2013 from Santa Teresa, NM.

Note: Figure 18 is provided courtesy of the Mesoscale and Microscale Meteorology (MMM) Division at the University Corporation for Atmospheric Research (UCAR) (34).

Figures 19 and 20 show the forecast for surface winds and the AFWA turbulence forecast using the 1.67-KM WRF over the LRU grid. While there is no cumulus parameterization applied at this horizontal grid spacing (1.67 km), the convection is well simulated by the model in both time and space. Additionally, the turbulence forecast follows the wind forecast almost precisely with an area of MOD and SEV turbulence forecasted in the region of 20-m/s wind along the border of Texas and Mexico. The second line of apparently high-based convection to the north near LRU is not as well simulated; however, there is still a small area of diverging surface winds just to the north of El Paso, TX, which gives some small signal that a weak downdraft or outflow may be simulated in the area. This area is only about 25 km from the radar echoes near LRU where locally strong winds were observed.

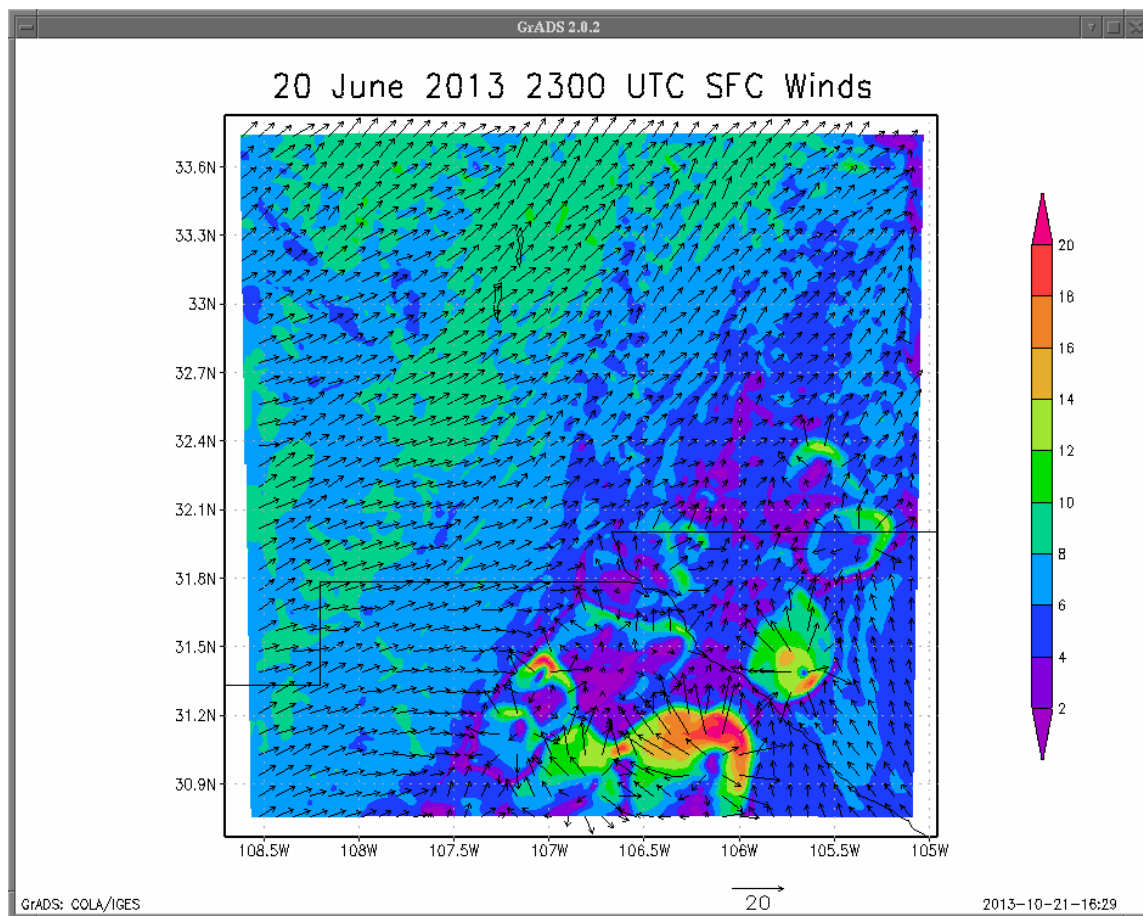


Figure 19. WRF 1.67-km forecast for surface winds at 2300 UTC on 20 June 2013.

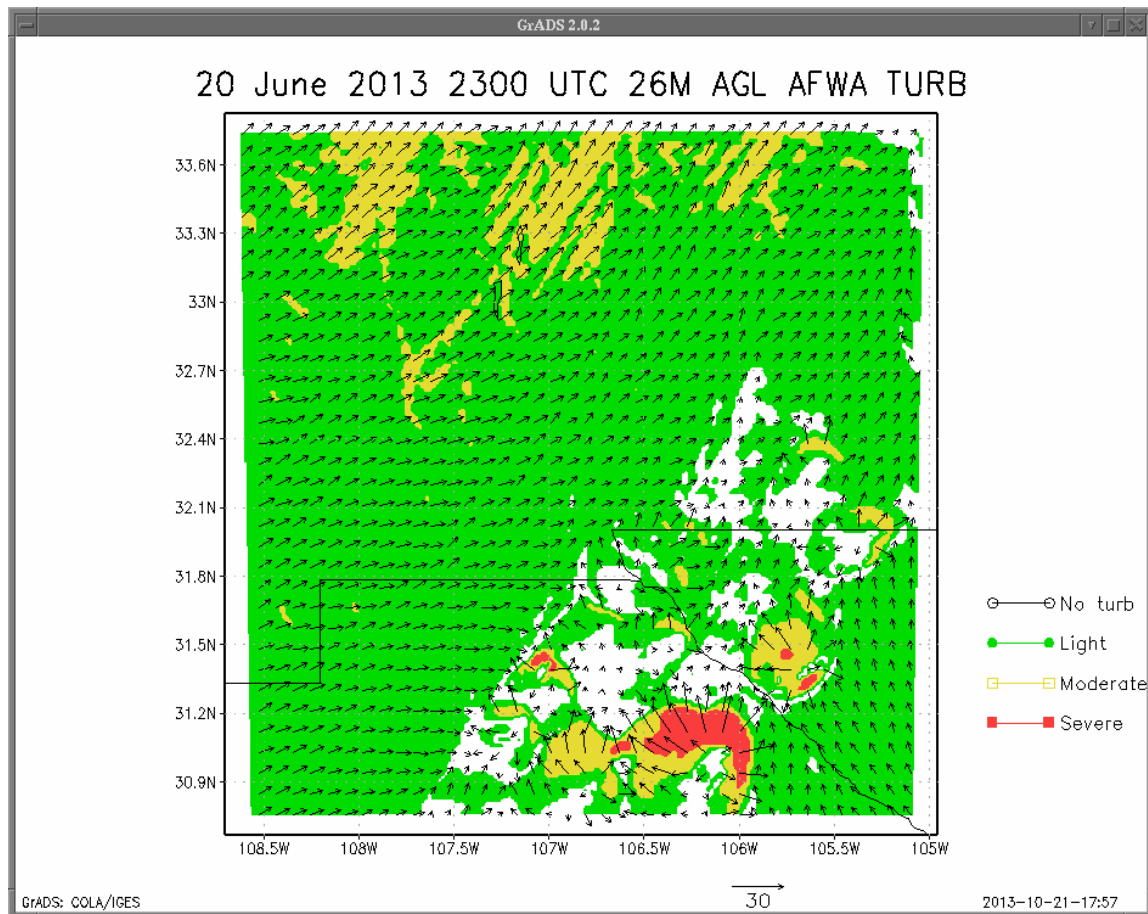


Figure 20. Turbulence forecast from AFWA routine at 26-m AGL (Level 2) for 20 June 2013 using WRF 1.67-km output over LRU grid.

While this case provides a very beneficial and useful forecast product, about 10 days later, another convective case did not. The 1 July 2013 case also had strong convective winds, with damage reported near Truth or Consequences, NM, and winds of 27 to 29 m/s in an area northwest and west of LRU. The 1 July 2013 case was slightly different than the 20 June 2013 case, since there was significantly more moisture through the atmospheric column (not shown). This was more typical of the summer monsoon in the desert southwest. Rather than producing a localized microburst, this appears to be a straight-line, long-lived outflow boundary or gust front that travelled a long distance for over an hour based on observations.

Figures 21 and 22 show the progression of the rain complex north to south across the valley. However, the model was unable to capture this feature as seen in figure 23 where the 0300 UTC model forecast indicates southerly flow across the region and no influence from convection in the valley. There is, however, some indication of a larger area of diffluent surface winds over the Gila Mountains to the northwest. The radar in figure 22 does indicate rainfall north of the region where the model is forecasting the outflow.

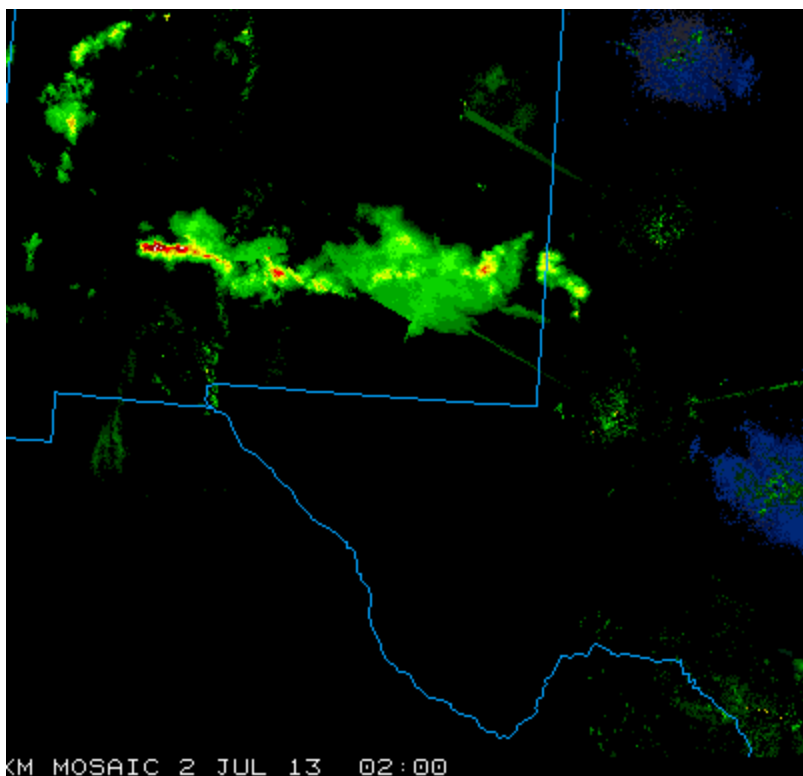


Figure 21. Santa Teresa, NM (EPZ) radar at 0200 UTC on 2 July 2013.

Note: Figure 21 is provided courtesy of the MMM division at UCAR (34).

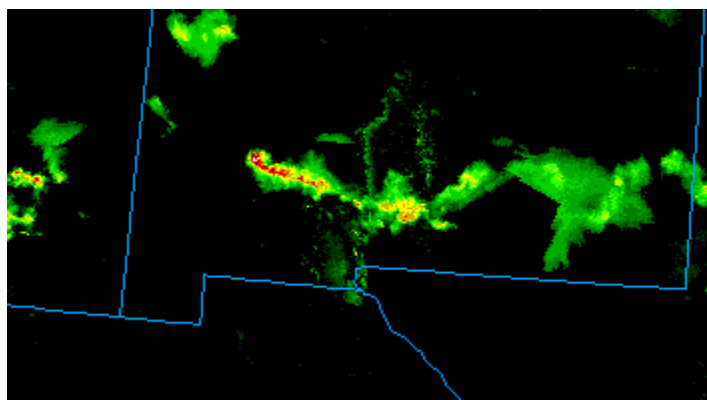


Figure 22. Santa Teresa, NM radar at 0259 UTC 2 July 2013.

Note: Figure 22 is provided courtesy of the MMM division at UCAR (34).

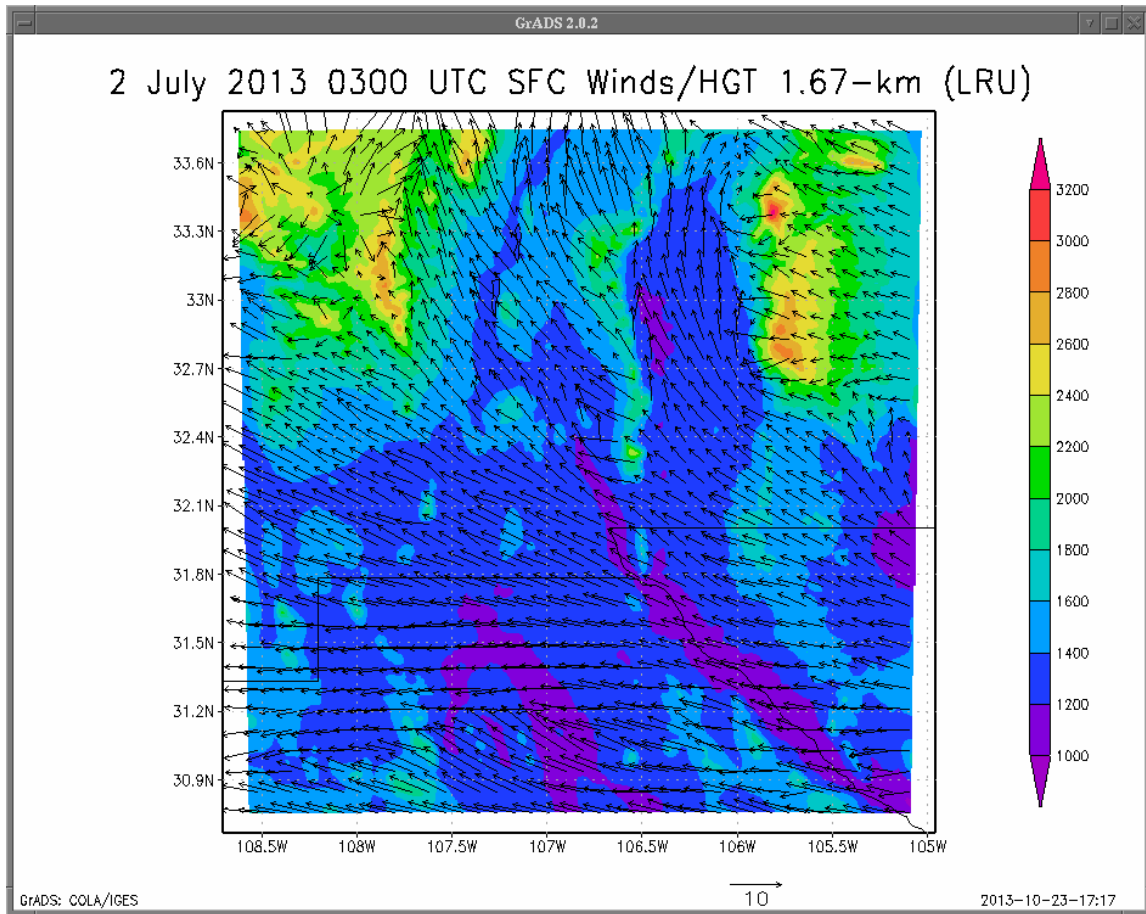


Figure 23. WRF 1.67-km surface wind forecast with terrain data at 0300 UTC on 2 July 2013.

Without the proper forecast of convection and the responding wind flow (figure 24), the turbulence forecast is based on using the PI and shows mostly areas of LGT turbulence across the grid; however, the turbulence forecast is “unaware” of the convective outflow and the resulting 29-m/s winds.

It is impossible to make any conclusions about the skill of the 1.67-km WRF or the turbulence forecast routines based on this small number of cases. While these cases are limited, they still do produce many encouraging results. In the first case, the 20 June 2013 case, the model does an excellent job of forecasting the high-based convection and resulting outflow winds, although they occur in regions where verification could not be accomplished due to lack of data and the scales involved. In the 1 July 2013 case, the model was not as successful in handling the more traditional summer monsoon case, but the ARL turbulence forecast and AFWA routine (not shown) did produce some signals of turbulence using the model output at 0300 UTC on 2 July 2013.

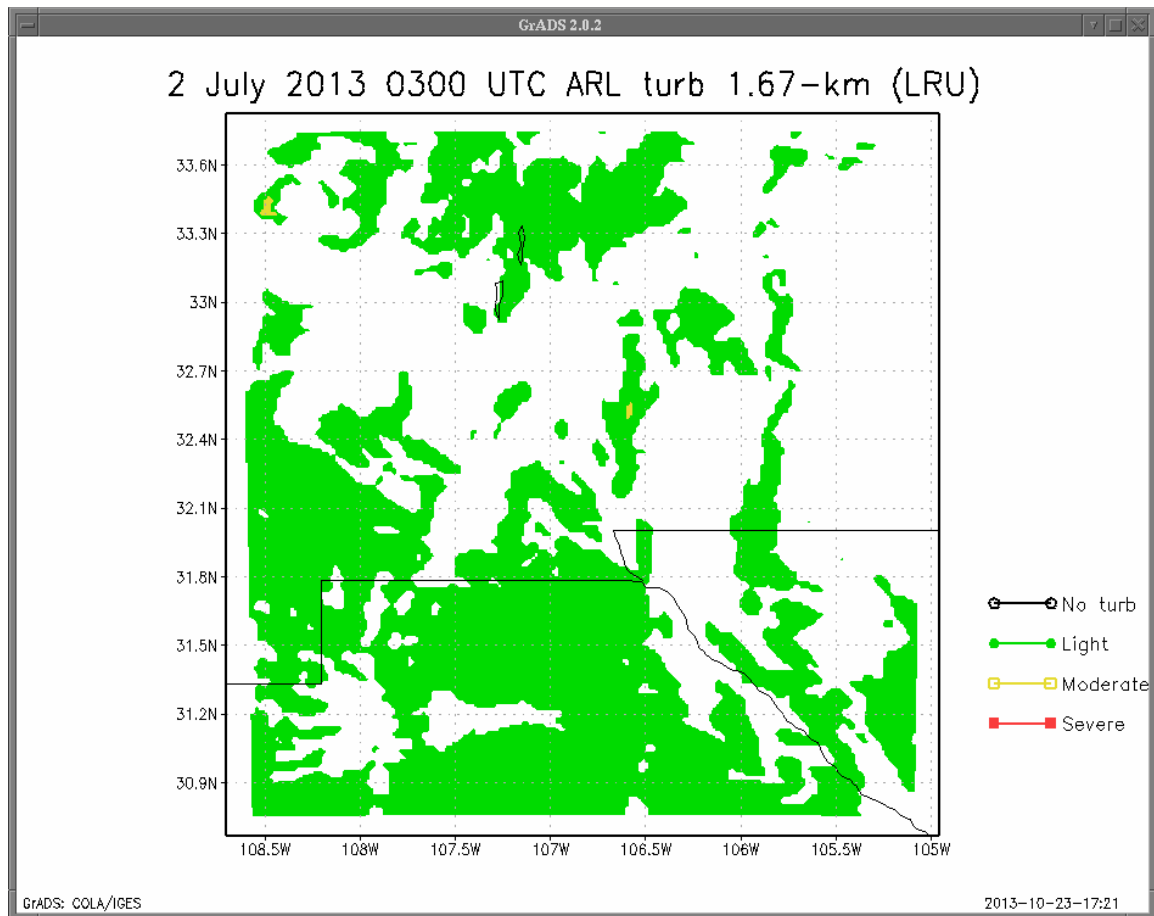


Figure 24. ARL turbulence forecast using WRF output at 0300 UTC on 2 July 2013.

### 5.3 Strong Down Slope Winds: 19 December 2012

The 19 December 2012 case over the LRU/White Sands Missile Range (WSMR), NM area featured very strong winds along with intense local downslope gusts as high as 38 m/s at 1500 UTC at WSMR's main post and 40 m/s on nearby San Augustin Pass (1800-m MSL). The 1200 UTC sounding at EPZ (figure 25) shows strong winds of 26 m/s just above the surface layer and mid-level winds between 36 and 49 m/s. This was a highly dynamical case where strong turbulence might be expected. However, the forecasted WRF 1500 UTC surface winds (figure 26) indicate strong surface winds on the mountain peaks but not at the base of the mountain where the 38 m/s winds were recorded. No effort to verify the turbulence forecast was attempted, due to a lack of PIREPs in the area; however, this was another case where the model and the related turbulence forecast did not capture the local turbulence at the lower levels as seen in figure 27.

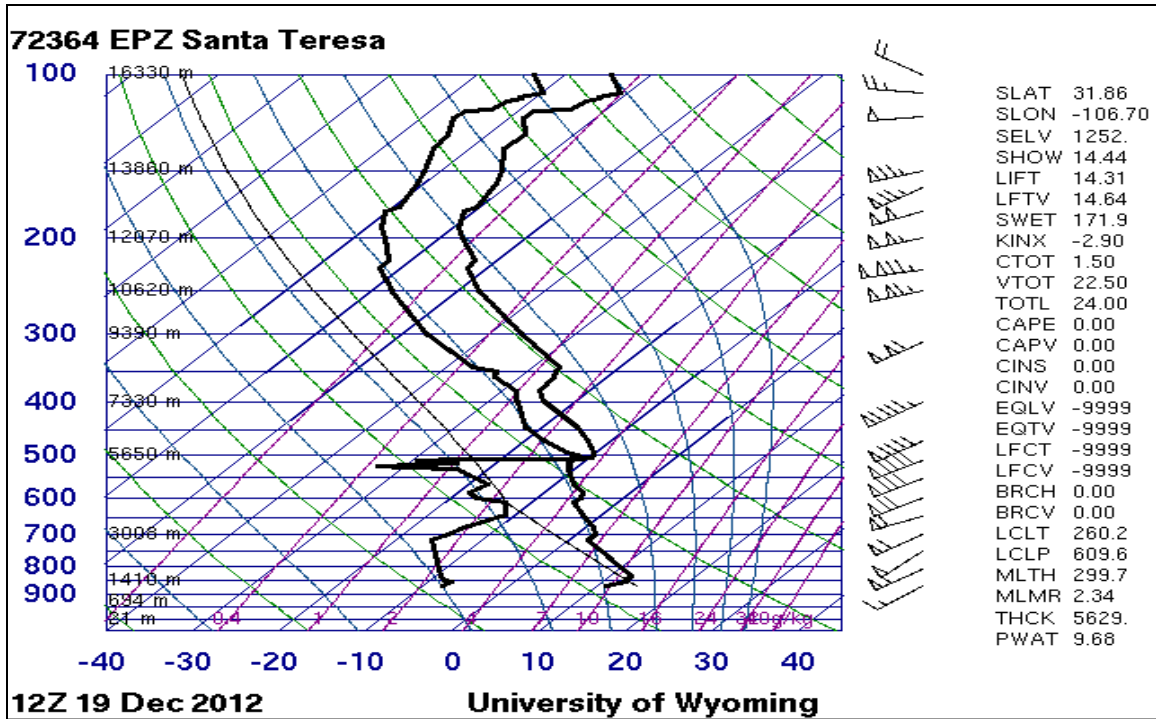


Figure 25. The 1200 UTC on 19 December 2012 sounding at EPZ.

Note: Figure 25 is provided courtesy of the University of Wyoming, Department of Atmospheric Sciences (31).

The plot indicates areas of MOD and some SEV turbulence in many areas of the grid; however, at the base of the Organ Mountains where WSMR is located, there were only areas of NONE or LGT turbulence forecasted.

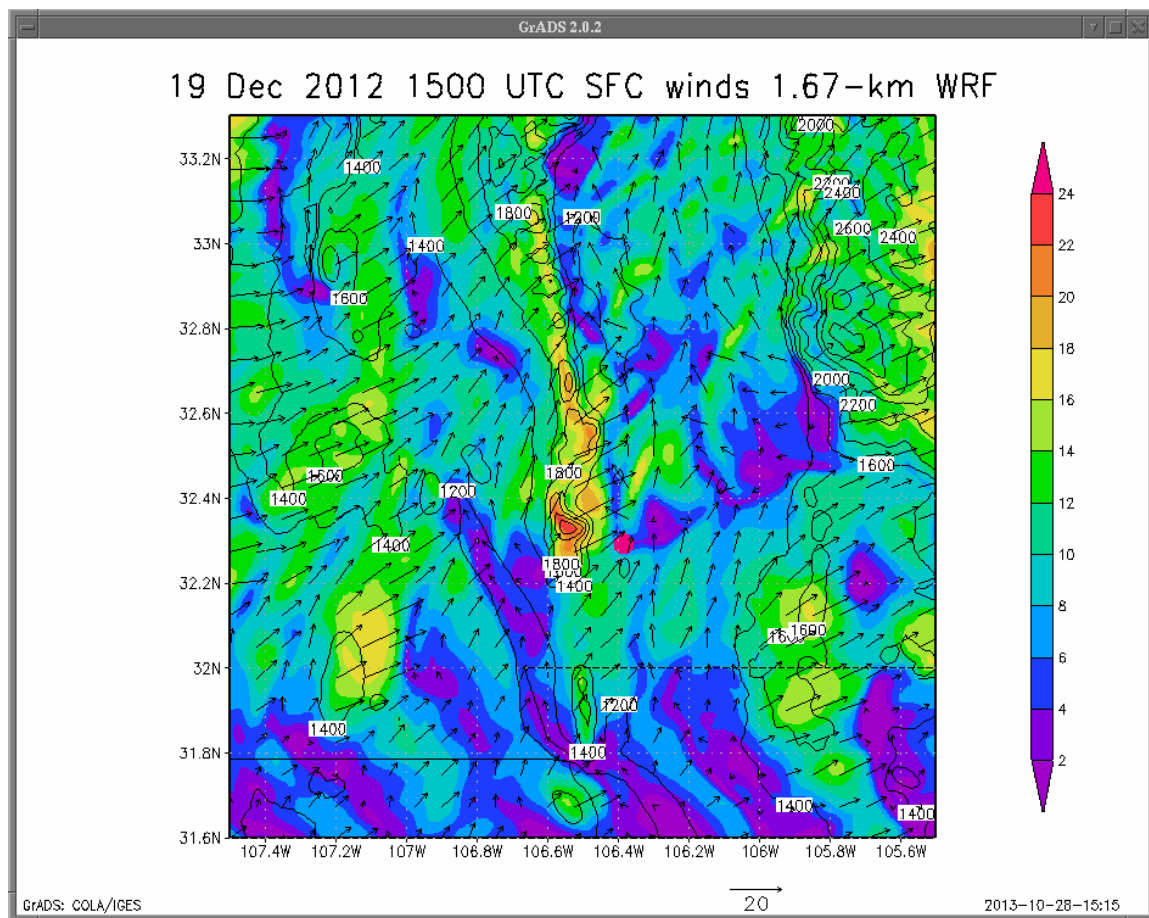


Figure 26. At 1500 UTC 1.67-km WRF surface wind forecast for 19 Dec 2012 over the LRU/WSMR grid.

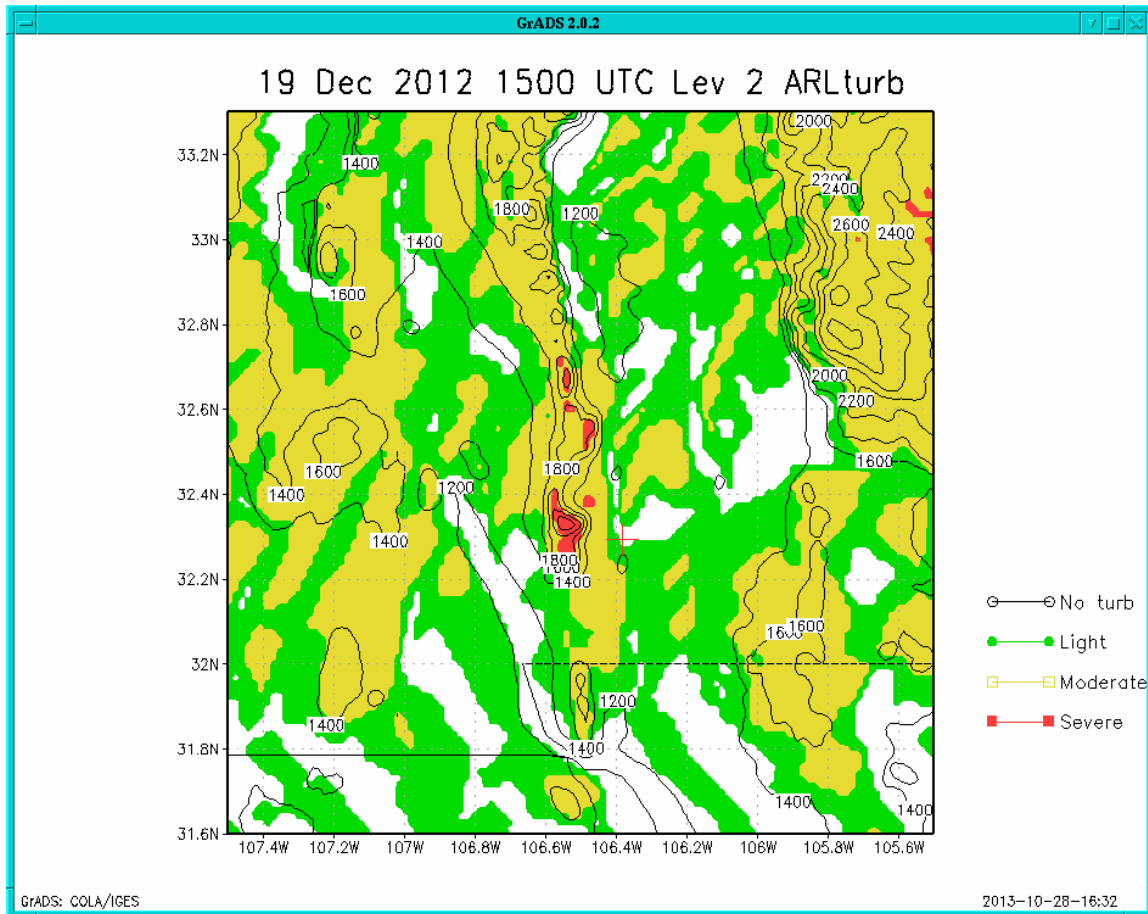


Figure 27. ARL forecast for turbulence using the 1.67-km WRF at 1500 UTC on 19 December 2012 over the Las Cruces/WSMR grid.

The model at 1500 UTC is predicting an easterly wind at the surface on the WSMR main post, which is represented by the red dot near 32.33° N and 106.34° W. The verified Surface Automated Measurement System winds data was 251° at 11 m/s with the peak gust of 38 m/s. At level 12 (not shown), which is at 279-m AGL, the model indicates a south winds (193°) at 11 m/s.

## 6. Discussion

Forecasting CAT or turbulence has evolved over the years. There have been plentiful attempts and efforts from many researchers who have applied numerous different methods to forecast CAT and turbulence. Some routines have been designed to solve specific issues related to turbulence such as gravity waves or mountain waves. While many of these packages are highly pertinent they are not directly related to the goals of ARL, which runs the WRF at 1-km

horizontal grid spacing and has a need for more frequent updates in time in order to develop more precise weather information in and near the boundary layer.

Much of the work related to turbulence forecasting has been designed for civilian aircraft which often fly above 6097 m for much of the flight. Sharman et al. (35) have developed the Graphical Turbulence Guidance (GTG), which is a statistical forecast that is based on the weighting of a set of previously used diagnostics determined to have the skill in CAT forecasting. The original GTG was used above 6097-m AGL and is for MOD or greater CAT. The Rapid Refresh Model, which is an hourly updated assimilation model operational at NCEP, uses a 13-km horizontal spacing and 50 vertical levels, has recent upgrades that might someday be useful for Army and Air Force applications and tactical decision aids. The recent version of GTG (V2.5) forecasts turbulence as low as 3354 m. Silberberg (36) notes that the Aviation Weather Center has recently adjusted the criteria for each category; LGT, MOD, SEV turbulence and this has improved forecast accuracy. Future versions of GTG may forecast turbulence down to the surface.

One of most challenging aspects of this present study was trying to observe, forecast, and verify turbulence that may influence the operation of aircraft in the boundary layer. UAS may fly at a variety of levels, but as has been learned here, there are so many dissimilar mechanisms that can generate turbulence in the boundary layer and above, that it is impracticable to separate them or truly understand the multiple interactions that occur. Thus, it remains an issue as to how to best approach the “turbulence problem.” For many years the chosen method at ARL and AFWA has been to use the PI, which accounts for buoyancy and wind flow into an explicit parameter. As models have advanced such features as terrain influences and radiation impacts have been included in the model feedbacks and model output. It is the opinion here, that individual routines to include terrain and radiation, for example, should not be necessary since it may be adequate to just “accept” the high-resolution model output as “fact” and then apply this to the existing turbulence routines.

A reality is that there are so many different methods and theories in development right now that it is impossible for them to answer all the questions and needs of turbulence forecasting. At some time in the future, the GTG may be mature enough and validated properly that it can fit a “one-for-all” approach to turbulence forecasting. However, at the current time, this is not possible so a continuation of multiple methods, and in many cases, different methods for different layers of the atmosphere remains as the possible “best technique.”

Still, this study has shown some of the major strengths and weaknesses in our current turbulence forecasting. The forecasts are highly dependent upon the model output, and while there are complex questions about the math, physics, and parameterizations of using a 1-km horizontal grid spacing, it has been determined that the turbulence routines tested in this study are adequate. However, this is especially true in obvious turbulence cases, but the models are not yet capable of resolving many mesoscale weather and terrain features that can influence the local wind,

moisture and thermal properties at these scales. Examples shown are strong down slope wind events, convection, and resulting outflow winds, and subcloud layer turbulence.

The original motivation of this research was the 7 April 2011 case over Afghanistan where four Aerostats were lost. The 1-km WRF was run after the event and figures 28 to 31 show a sequence of forecasts from 1500 to 1800 UTC at level 9 (approximately 284-m AGL). Each plot presents the forecasted wind direction and forecasted turbulence field (shaded) at level 9 using the 1-km WRF output. This model simulation was conducted with a  $121 \times 121$  horizontal grid points using 90 vertical levels.

The model output in this 7 April 2011 case indicates a wind shift or outflow boundary caused by high-based convection on this day. In the initial panel at 1500 UTC (figure 28) the flow at level 9 is basically undisturbed and light from the west. The outflow boundary is just entering the western edge of the grid. By 1600 UTC (figure 29) the strong windshift line has progressed across the northern part of the grid and this trend continues at 1700 UTC (figure 30). The shaded areas of green and yellow colors show where the forecast is for LGT and MOD turbulence respectively. By 1800 UTC (figure 31) the boundary has progressed across the entire domain and the wind speed on the grid has decreased.

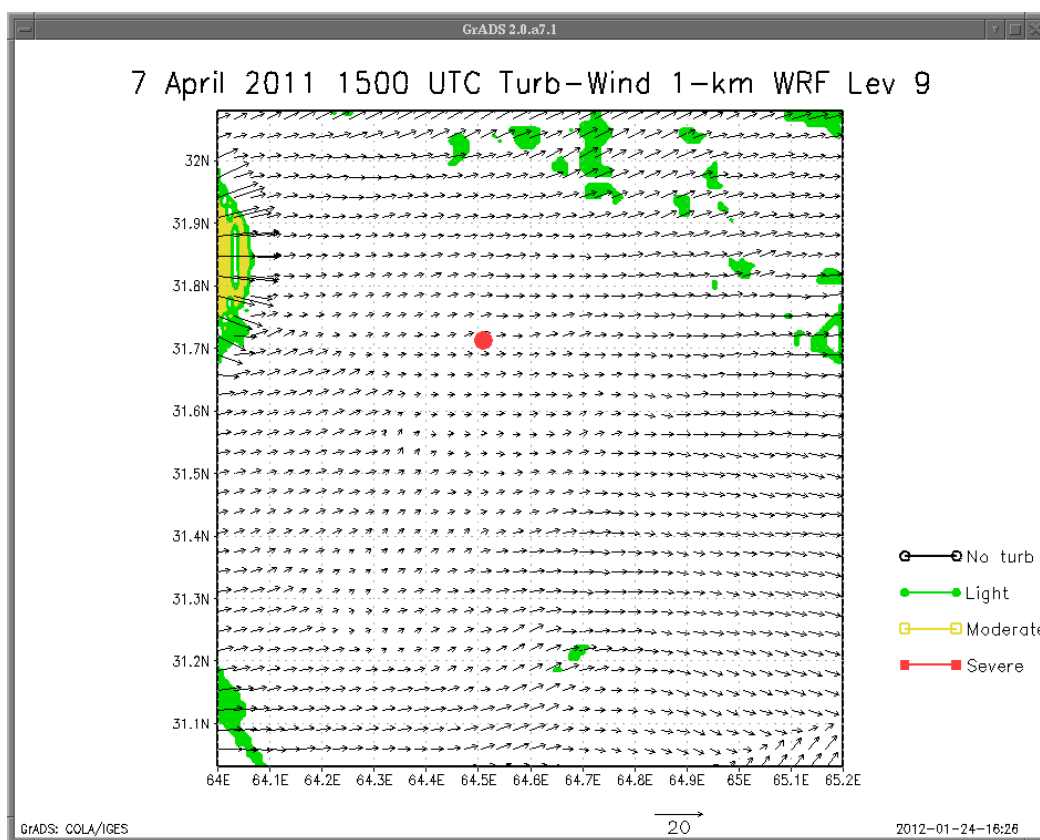


Figure 28. On 7 April 2011, the 1500 UTC plot of 1-km WRF winds and forecasted turbulence using the ARL routine at level 9, which is the approximate level of where the Aerostat was flying. The red dot is at a location where one of the Aerostats was lost.

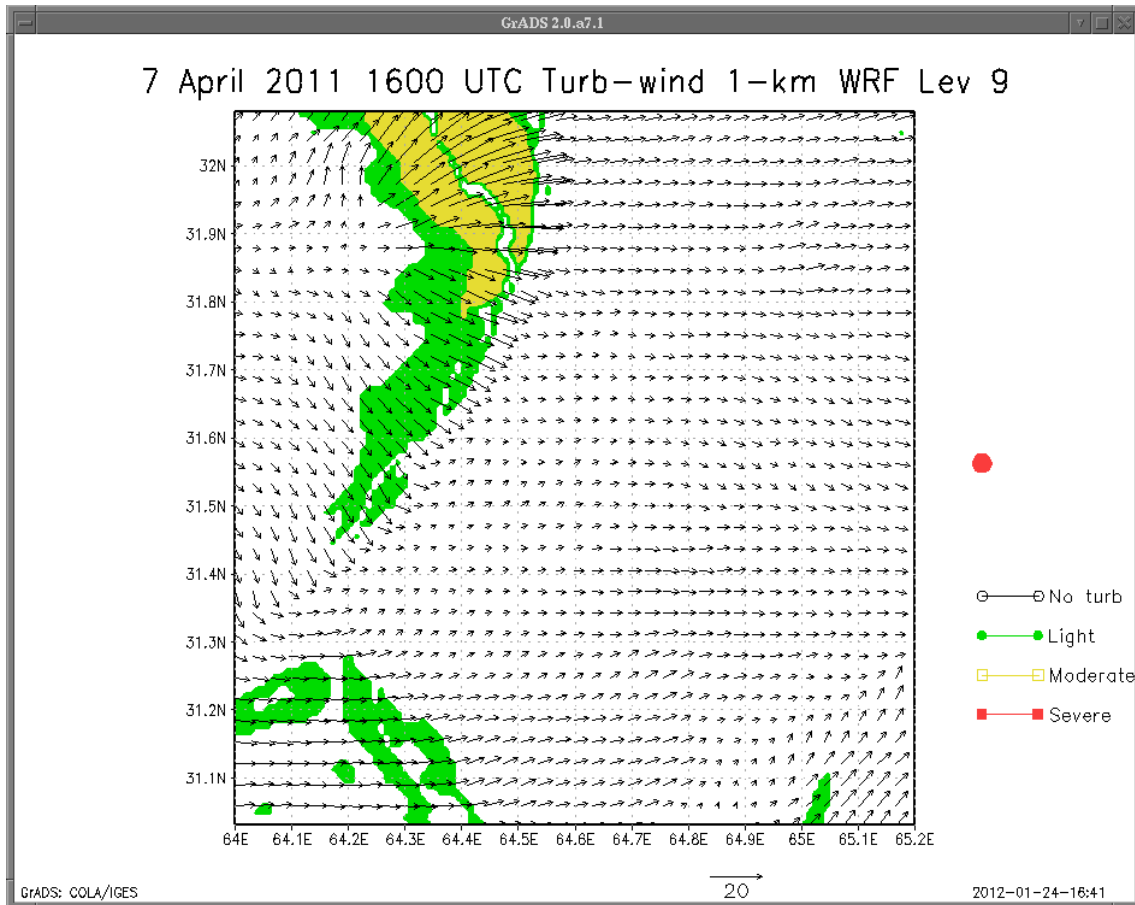


Figure 29. On 7 April 2011, the 1600 UTC plot of 1-km WRF winds and forecasted turbulence using the ARL routine at level 9, which is the approximate level of where the Aerostat was flying.

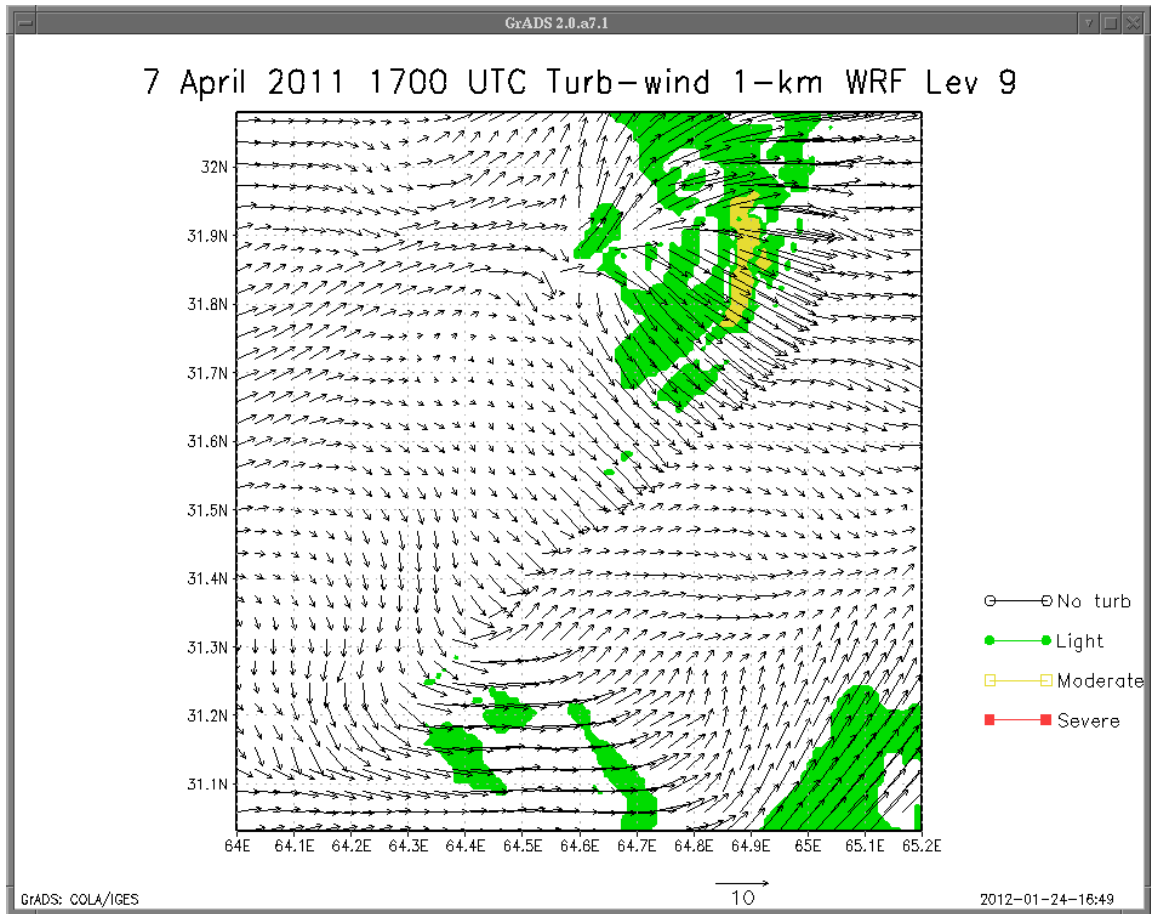


Figure 30. On 7 April 2011, the 1700 UTC plot of 1-km WRF winds and forecasted turbulence using the ARL routine at level 9, which is the approximate level of where the Aerostat was flying.

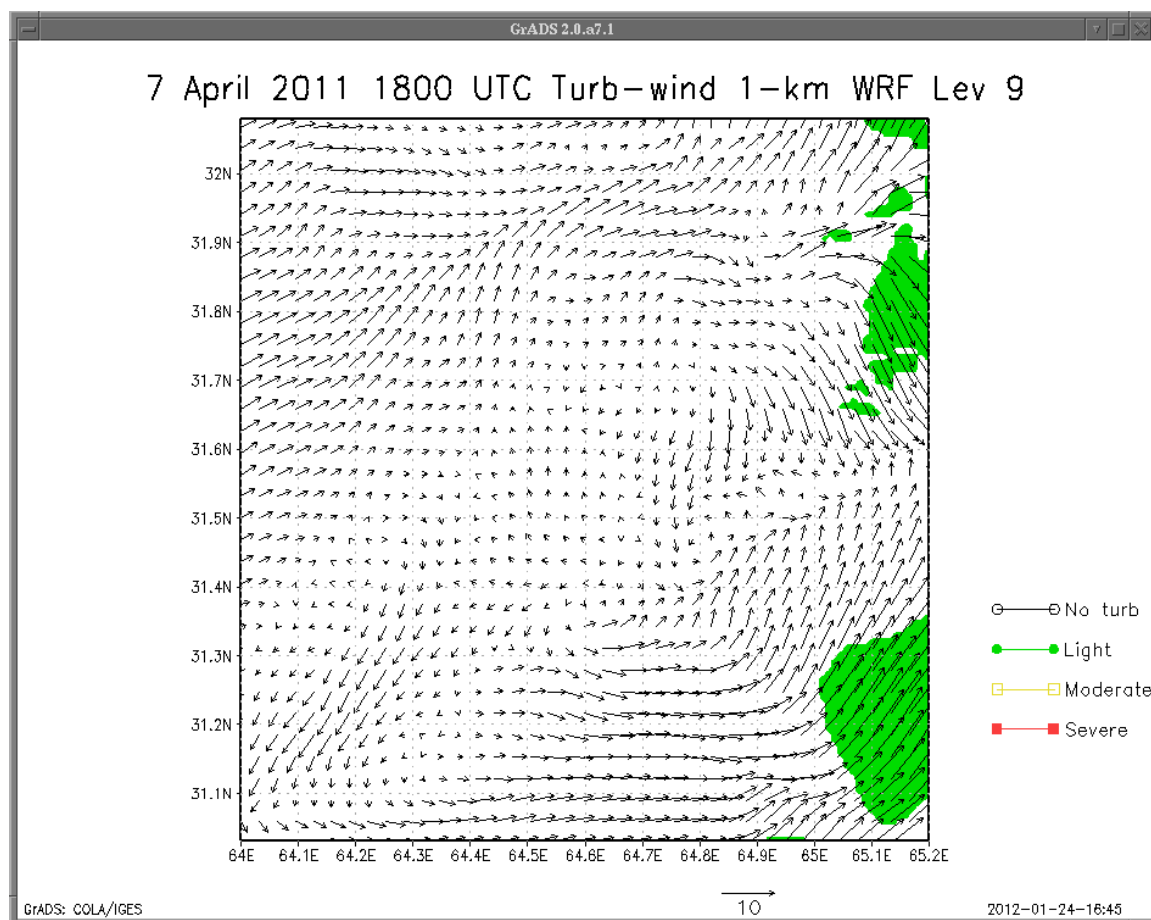


Figure 31. On 7 April 2011, the 1800 UTC plot of 1-km WRF winds and forecasted turbulence using the ARL routine at level 9, which is the approximate level of where the Aerostat was flying.

While surface observations are characteristically very limited in Afghanistan, from 1416 UTC to 1700 UTC, available observations indicate that a wind shift and increasing wind speeds occurred. Forward Operating Base (FOB) Dwyer located at 31.1° N 64.08° E reported a wind shift from 070° to 270° at 1416 with an increase of winds to 10 m/s with a gust to 15 m/s. Table 10 shows the sequence of surface observations from 1300 UTC to 1600 UTC at this location

Table 10. Observations from 1300 to 1600 UTC on 7 April 2011 at FOB Dwyer, Afganistan 31.10° N 64.08° E (725-m elevation).

Time (UTC)	Temp (°C)	Dew Point (°C)	Wind Dir (°)	Wind Speed (m/s)
1300	28	-3	070	4
1416	22	11	270	10G15
1440	22	10	270	8G15
1500	22	11	290	11G15
1515	21	11	280	7G15
1600	22	9	060	6G8

Other reporting stations such as FOB RAMROD located at 31.63° N 64.95° E (not shown) also indicated a wind shift and reported wind gusts to 13 m/s at 1600 UTC with an increase in dew point to 12 °C. FOB Pasab/Wilson at 31.58° N 65.43° E also showed winds gusting to 13 m/s at 1700 UTC with a dew point increase from 0 to 10 °C.

In this study it was found that an additional parameter for meteorologists to study for predicting turbulence may be the MYJ TKE taken directly from the model. Figure 32 shows the plot of TKE at 1600 UTC at level 9 from the 1-km WRF output. The highest levels of TKE are located in the northwest part of the grid and this is in good agreement with figure 29, which displays the turbulence forecasts using the ARL method and is also in agreement with the AFWA forecast (not shown).

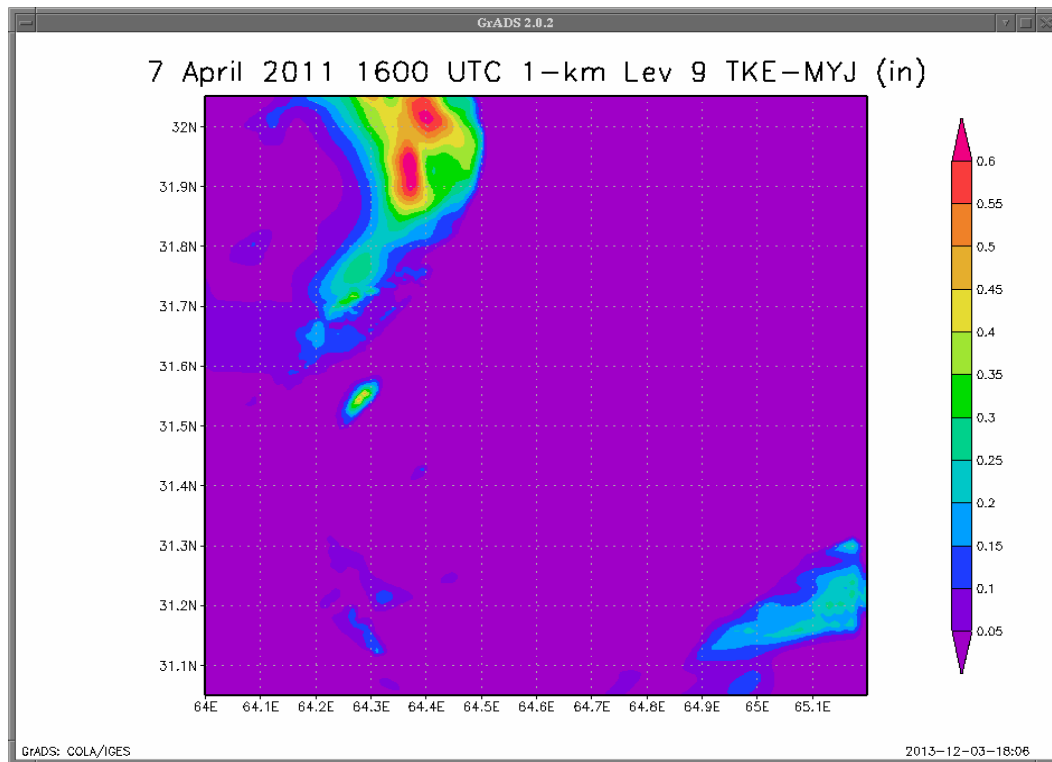


Figure 32. On 7 April 2011, the 1600 UTC plot of 1-km WRF-derived MYJ TKE at level 9, which is the approximate level of where the Aerostat was flying.

It is encouraging that the model can resolve convective outflow explicitly as in the 7 April 2011 case. The turbulence forecasts provide guidance that can give the needed warning on a short-term basis for low-flying and vulnerable aircraft. However, as seen in this study, the models do not accurately forecast such conditions in all cases as there are predictability issues in timing and spatial resolution of these structures and features.

As McCormick (27) points out, despite the efforts of the forecasting and research community there are no comprehensive methods for forecasting all turbulence types and intensities. However, in this study several ideas have been presented that may upgrade our ability to forecast turbulence. A listing appears below:

- Increasing the vertical resolution in the lower levels and at typical inversion levels (if known) will assist in model improvement.
- Improving convective forecasts will enhance the turbulence routines. Often the downdrafts are far more damaging than the updrafts and cannot be detected with much advanced warning.
- The turbulence routines examined in this study are valuable in forecasting the “YES” and “NO” forecasts, but turbulence intensity remains a multifaceted issue and the effects vary greatly from aircraft to aircraft. In the future, it may be necessary to adapt the turbulence forecasts for particular aircraft or missions to gain more precise forecasts.
- Adjusting the model microphysics (using other microphysics schemes) may be helpful in determining layers of small-scale turbulence, which can cause strong local downdrafts.
- There are very few studies of turbulence routines during the nighttime hours. This area has been neglected because of lack of verification/PIREPs at night. Commercial aviation is greatly reduced at night, but military missions often take place at night.
- It may be advantageous to reduce the effort for individual routines that forecast gravity waves, mountain waves, and other causes of turbulence. These problems are difficult to understand or solve, but it might be more economical to improve the models. As seen in the 16 February 2013 case, the turbulence routines can be very effective, but the routines are model dependent.
- Most of the turbulence routines do not account for wind gusts, which can cause major damage to aircraft.

The final suggestion in this study would be to implement additional data types and data into the mesoscale models to improve the forecasts through data assimilation. Four-dimensional data assimilation (FDDA) is a technique where forecast values are nudged toward the observation in an effort to improve forecast quality and performance by inserting local or regional observed weather through additional relaxation or artificial “forcing” terms. This is particularly a powerful tool in data-void regions where surface and upper-air data are typically not available. However, it is also useful in data-rich areas because it acts to make corrections and improve the model output (37).

In this new experiment, the observations were ingested during the model run using a continuous, dynamic assimilation method. Vital to the weight parameters, is the radius of influence in the horizontal and vertical, the time window, and nudging coefficient, which are all set in the

model's input file. Observations from the Meteorological Assimilation Data Ingest System (MADIS) were used for data assimilation. The MADIS data included standard surface observations, as well as mesonet data, maritime observations, profiler data, aircraft data, and rawinsondes. Figure 33 shows the turbulence forecast using FDDA on 7 February 2012 over the California grid while figure 34 displays the turbulence forecast over domain 3 without the data assimilation.

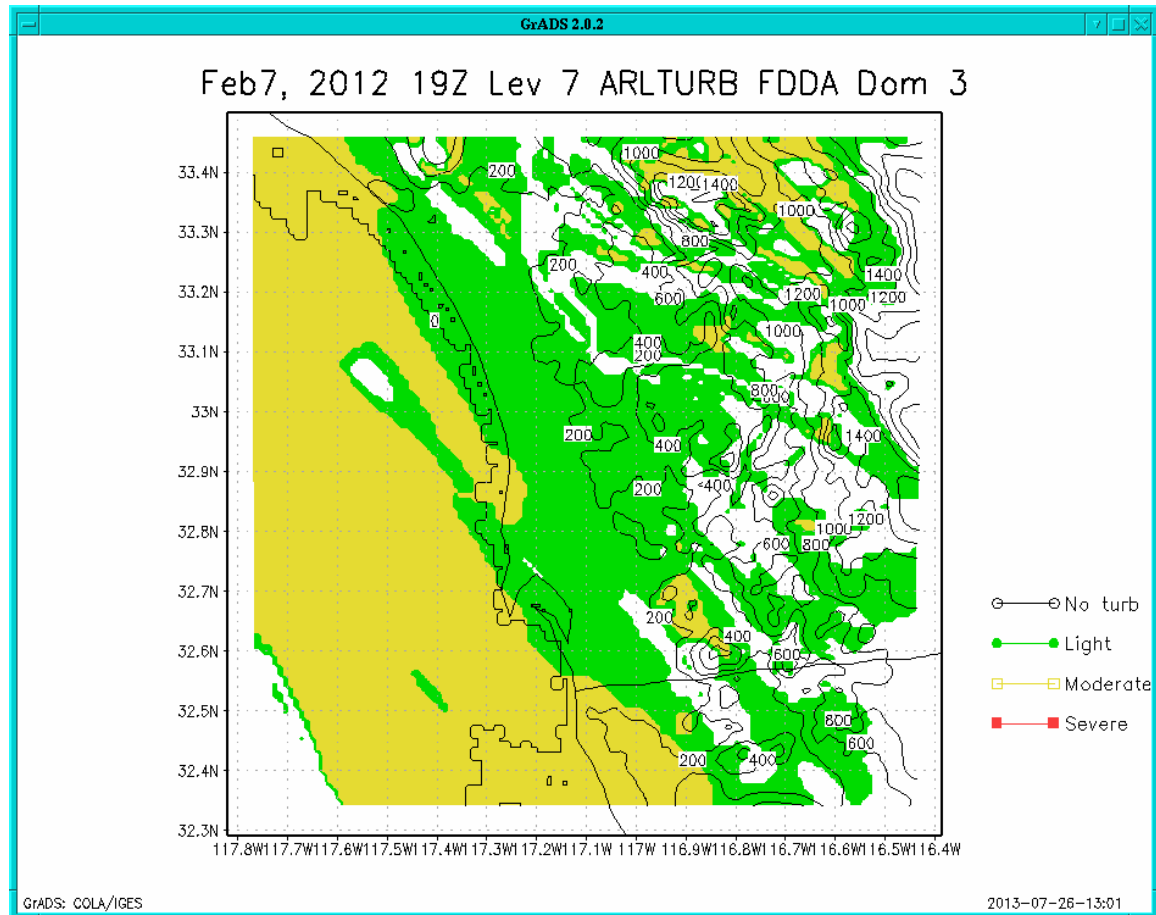


Figure 33. On 7 February 2011, the 1900 UTC (level 7) 1-km turbulence forecast with FDDA included. Elevation (m) is plotted in the contoured over the domain.

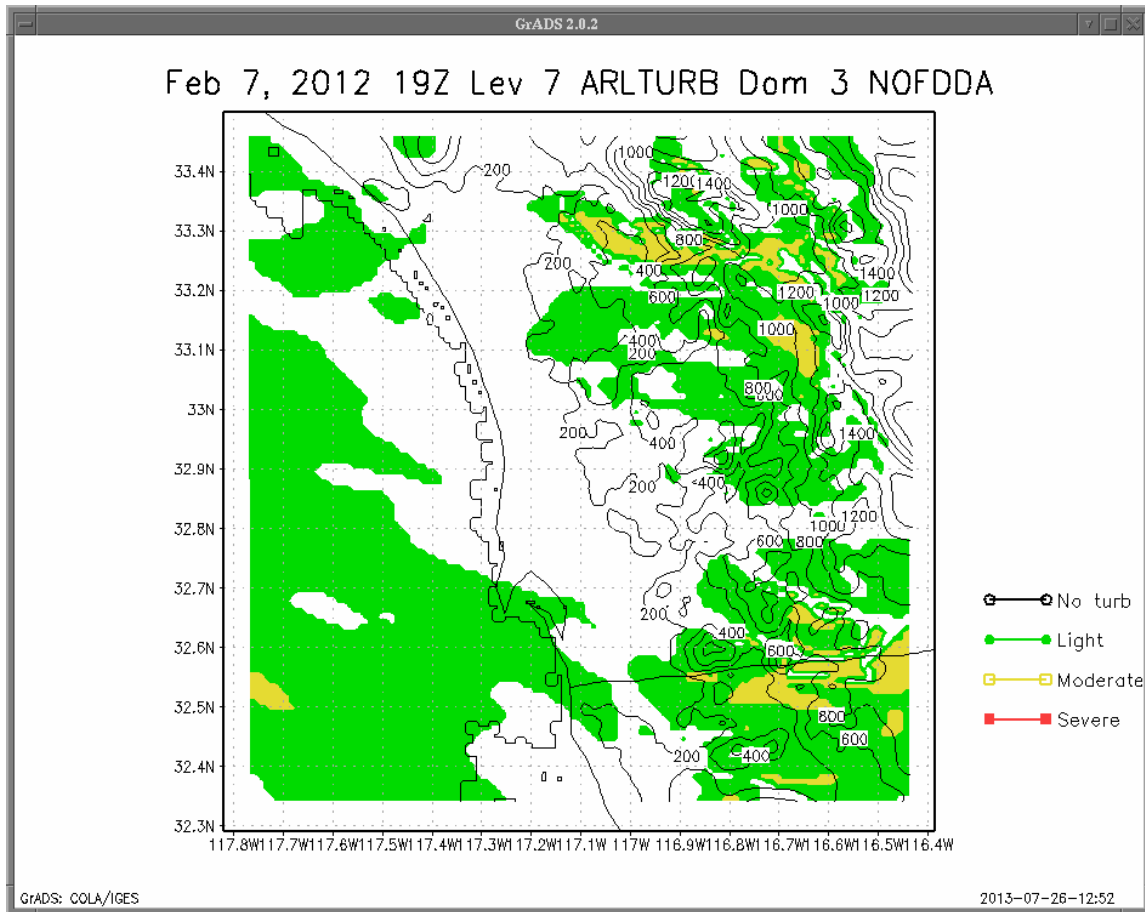


Figure 34. On 7 February 2011, 1900 UTC plot (level 7) of 1-km turbulence forecast without FDDA. Elevation (m) is plotted in contours over the domain.

## 7. Conclusions

In February 2013 there were six incidents in which aerostats “crashed due to wind.” Strong winds, downdrafts, lightning, and precipitation can damage or destroy aerostats. ARL, with an emphasis on fine-resolution, short-range forecasts ran the WRF with three nests of 9-, 3-, and 1-km grid spacing over a 24-h period. The main emphasis in this study was using the WRF model output to produce a postprocessed turbulence forecast using four different software routines as well as using the explicit model TKE from the MYJ scheme.

It was determined to study some existing methods that had an emphasis on the boundary layer and the lower-levels of the atmosphere. Methods from AFWA, ARL, UPP, BLTURB routine, and the MYJ TKE forecasted by the WRF were tested for five different meteorological days where PIREPs were collected. Overall, the routines from AFWA, ARL, and UPP showed similar tendencies—high POD, low FAR, and a distinct difficulty in forecasting the nonevent case with

all three routines having the same correct nonevent skill of 0.44% or 44%. The ARL method showed the best skill in determining the turbulence intensity with 35% accuracy; however, it is uncertain how significant the intensity forecasts are. The BLTURB had the lowest skill and was limited in the number of available samples since it is only used from the surface to the height of the WRF-calculated PBL. It appears that the BLTURB skill level was hindered by using the WRF 1-km output, which this original work was not designed for. The MYJ TKE from the WRF showed excellent skill in forecasting the “YES/NO” turbulence forecast. This method has not been thoroughly tested and it also requires the user to use the MYJ PBL in the model’s input file to get any results of the method.

Another aspect of this study was to investigate new methods or ideas to improve the turbulence forecasts with an emphasis on the boundary level where most of the Aerostats were destroyed. To help solve this costly problem, it may be best to greatly increase the number of vertical levels near the surface, with an additional increase at or near inversion levels. Improving convective forecasts or perhaps a study of model microphysics to find the best parameterization to apply in convective cases should be investigated. The microphysics and vertical motion approach can also be very useful in forecasting turbulence that forms underneath a cloud base particularly in small layers with steep lapse rates. Additionally, studies of turbulence at night are lacking, and this should be a future area of study for military applications. The current routines only use wind speeds and not wind gusts, which can cause damage to low-flying aircraft or exposed air craft on the ground.

Finally, model enhancement should dramatically assist in improving forecasts in all areas, and it is felt that superior wind fields and temperature fields should provide better forecasts of CAT and turbulence. It will also be interesting to study what model resolution is a reasonable limit for a skillful forecast of a parameter such as turbulence. The future path at ARL is to continue to advance the WRF model by adding additional data sources through data assimilation. Studies at ARL will continue to statistically evaluate how the observation nudging influences model simulations. Future work will also investigate additional methods of observation nudging and other techniques that can enhance model performance at these high resolutions. It is hoped as models gradually perform better, meteorologists can gather more clues on low-level turbulence formation and intensity, and provide more consistent forecasts of the temperature, winds, and moisture fields that all contribute to create turbulence. Obviously, it is the “big picture” that influences the “small picture” so additional development in model initialization and model physics will also serve to provide superior model output.

It is realistic that this process is a gradual one. This is a “two-way” street; improving the model will advance our understanding of the mass and momentum fields in the boundary and how they interrelate with the local terrain. Similarly, understanding the processes involved in turbulence formation will improve the models. Great strides have already been made and more can be made through the work presented here.

---

## 8. References

---

1. Wikipedia. <http://en.wikipedia.org/wiki/Aerostat> (accessed 24 July 2013).
2. Public Radio East.  
<http://www.publicbroadcasting.net/pre/news.newsmain/article/1/0/1950743/ENC.Regional.News/A.Look.at.Theethered.Aerostats> (accessed 24 July 2013).
3. Defense News.  
<http://www.defensenews.com/article/20130507/C4ISR02/305070027/Aerostats-Lost-Weather-Mishaps-Take-Heavy-Toll-Dirigibles> (accessed 18 July 2013).
4. Skamarock, W. C.; Klemp J. B.; Dudhia, J.; Gill, D. O.; Barker, D. M.; Duda, M. G.; Huang, X-Y; Wang, W.; Powers, J. G. *A description of the Advanced Research WRF version 3*; NCAR Tech Note NCAR/TN-475+STR; National Center for Atmospheric Sciences: Boulder, CO, 2008.
5. Deng, A. D., Update on WRF-ARW end-to-end multi-scale FDDA system, *10<sup>th</sup> WRF Users' Workshop*, National Center for Atmospheric Sciences: Boulder, CO, June 23–26, 2009, Paper 1.9.
6. U.S. Army Research Laboratory Major Shared Resource Center. <http://www.arl.hpc.mil> (accessed 01 August 2013).
7. Gemmill, W. B.; Katz, B; Li, X. Daily Real-Time, Global Sea-Surface Temperature. NOAA/NWS/NCEP/MMAB office note 260, 2007.
8. National Operational Hydrologic Remote Sensing Center.  
[http://www.nohrsc.noaa.gov/archived\\_data](http://www.nohrsc.noaa.gov/archived_data) (accessed 16 December 2013).
9. Janic, Z. I. *Nonsingular Implementation of the Mellor-Yamada Level 2.5 Scheme in the NCEP Meso Model*; NCEP Office Note, No. 437, 2002, 61 pp.
10. Lee, J. A.; Kolczynski, W. C.; McCandless, T. C.; Haupt, S. E. An Objective Methodology for Configuring and Down-Selecting an NWP Ensemble for Low-Level Wind Prediction. *Mon. Wea. Rev.* **2012**, 140, 2270–2286.
11. Reen, B. P.; Dumais, R. E.; Passner, J. E. *Mitigating Excessive Drying from the Use Of Observations in Mesoscale Modeling*; U.S. Army Research Laboratory: White Sands Missile Range, NM, 2013 (unpublished).
12. Wikipedia. [http://en.wikipedia.org/wiki/Turbulence\\_kinetic\\_energy](http://en.wikipedia.org/wiki/Turbulence_kinetic_energy) (accessed 24 July 2013).

13. Dutton, J.; Panofsky, H. A. Clear Air turbulence: A mystery may be unfolding, *Science*, **1970**, *167*, 937–944.
14. Bacmeister, J. T.; Newman, P. A.; Gary, B. L.; Chan, K. R. An algorithm for forecasting mountain wave-related turbulence in the stratosphere, *Weather and Forecasting*, **1984**, *9*, 241–253.
15. Keller, J. L. Clear air turbulence as a response to meso- and synoptic-scale dynamic processes. *Mon. Wea. Rev.*, **1990**, *118*, 2228–2242.
16. McCann, D. W. An Evaluation of clear-air turbulence indices. Preprints of *5<sup>th</sup> International Conference on Aviation Weather Systems*, Vienna, VA, 1993, Paper 8.2.
17. Miles, J. W.; Howard, L. N. Note on a Heterogeneous Shear Flow, *J. Fluid Mech*, **2007**, *20*, 331–336.
18. Stull, R. B. *An Introduction to Boundary Layer Meteorology*, Kluwer Academic Publishers, Boston, MA, 1989, p 670.
19. Boyle, J. S. 1990: Turbulence Indices Derived From FNOC Field and TOVS Retrievals, Naval Oceanographic and Atmospheric Research Laboratories, NOARL Technical Note 47.
20. Ellrod, G. P.; Knapp, D. I. An Objective Clear Air Turbulence Forecasting Technique Verification and Operational Use. *Wea. Forecasting*, **1992**, *7*, 150–165.
21. Passner, J. E. *An Evaluation of the Three-Dimensional Weather Hazards Using Sounding Data and Model Output Data*; ARL-TR-1046; U.S. Army Research Laboratory: White Sands Missile Range, NM, 2000.
22. Knapp, D. I.; Smith, T. J.; Dumais, R. E. Development and Verification of a Low-Level turbulence Analysis and Forecasting Index Derived from Mesoscale Model Data, Preprint of *Sixth Conference on Aviation Weather Systems*, Dallas, TX, 1995, Paper 11.11.
23. Passner, J. E. *Using the Advanced Research Version of the Weather Research and Forecasting (WRF-ARW) to Forecast Turbulence at Small Scales*; ARL-TR-4575; U.S. Army Research Laboratory: White Sands Missile Range, NM, 2008.
24. Passner, J. E.; Dumais, R. E.; Flanigan, R.; Kirby, S. *Using the Advanced Research Version of the Weather Research and Forecast Model in Support of ScanEagle Unmanned Aircraft System test Flights*; ARL-TR-4746; U.S. Army Research Laboratory: White Sands Missile Range, NM, 2009.
25. Brooks, G. R.; Gotchel, I.; Stock, C. M.; Passner, J. E.; Knapp, D. I. Verification Results of a Turbulence Index Applied to Low-Levels of the Atmosphere. *10<sup>th</sup> Conference on Aviation, Range, and Aerospace Meteorology*, Portland, OR, 2002, Paper 9.3.

26. McCormick, J. R. Near Surface Forecast Challenges at the Air Force Weather Agency. *15<sup>th</sup> Conference on Aviation, Range, and Aerospace Meteorology*. Los Angeles, CA, 2011, Paper 3.5.
27. McCormick, J. R., Distributions Used in the Development of a Low-Level Turbulence Algorithm. *16<sup>th</sup> Conference on Aviation, Range, and Aerospace Meteorology*. Austin, TX, 2013, Poster 259.
28. McCann, D. W. Gravity Waves, Unbalanced Flow, and Aircraft Clear Air Turbulence. *Natl Weather Dig* **2001**, 25, 3–14.
29. Zhou, B. Personal Communications, 16 July 2013.
30. Olson, J. B.; Brown J. M. A comparison of Two Mellor-Yamada Based PBL Schemes in Simulating a Hybrid Barrier Jet. *23<sup>rd</sup> Conference on Weather Analysis/19<sup>th</sup> Conference on Numerical Weather Prediction*, Omaha, NE, 2009; JP1.13.
31. University of Wyoming. Department of Atmospheric Sciences.  
<http://weather.uwyo.edu/upperair/sounding.html> (accessed September 2013).
32. National Center for Environmental Prediction, Hydrometeorological Prediction Center.  
[http://www.hpc.ncep.noaa.gov/dailywxmap/index\\_20120216.html](http://www.hpc.ncep.noaa.gov/dailywxmap/index_20120216.html) (accessed September 2013).
33. DCDBS. Satellite Inventory. <http://dcdbs.ssec.wisc.edu/inventory/> (accessed September 2013).
34. MMM/UCAR. <http://www.mmm.ucar.edu/imagearchive/> (accessed October 2013).
35. Sharman, R. et al. An Integrated Approach to Mid- and Upper-Level Turbulence Forecasting. *Wea Forecasting*, **2006**, 21, 268–287.
36. Silberberg, S. Personal Communications, Nov 2013.
37. Pattantyus, A. Optimizing Strategies for an Observation-Nudging-Based Four-Dimensional Data Assimilation Forecast Approach with WRF-ARW. *Science and Engineering Apprenticeship Program*, Adelphi, MD, August 2011. (Unpublished).

---

## List of Symbols, Abbreviations, and Acronyms

---

AFWA	U.S. Air Force Weather Agency
AGL	above ground level
ARL	U.S. Army Research Laboratory
BED	Battlefield Environment Division
BLTURB	boundary-layer turbulence
CAT	clear-air turbulence
CVG	convergence
DCDBS	Digital Cadastral Databases
DEF	deformation
DFW	Dallas/Fort Worth International Airport
EPZ	Santa Teresa, NM
FAR	False Alarm Rate
FDDA	four-dimensional data assimilation
FNMOC	U.S. Navy Fleet Numerical Meteorological and Oceanography Center
FOB	Forward Operating Bases
GFS	Global Forecast System
GTG	Graphical Turbulence Guidance
HOTMAC	Higher Order Turbulence Model for Atmospheric Circulations
LAX	Los Angeles International Airport
LGT	“light” turbulence
LRU	Las Cruces International Airport
MADIS	Meteorological Assimilation Data Ingest System
MMM	Mesoscale and Microscale Meteorology
MOD	“moderate” turbulence

MSL	mean sea level
MYJ	Mellor-Yamada Janjić
NCEP	National Centers for Environmental Prediction
NONE	“no” turbulence
NWP	Numerical Weather Prediction
NWS	National Weather Service
OKX	Upton, NY
PBL	Planetary Boundary Layer
PI	Panofsky index
PIREPs	Pilot Reports
POD	Probability of Detection
qcloud	cloud water mixing ratio
RH	relative humidity
RI	Richardson number
SEV	“severe” turbulence
TI	Turbulence index
TKE	turbulent kinetic energy
TSS	True Skill Score
UAS	unmanned aircraft systems
UCAR	University Corporation for Atmospheric Research
UPP	Unified Post Processor
UTC	Coordinated Universal Time
VWS	vertical wind shear
WPP	WRF Post Processor
WRF	Weather Research and Forecasting
WRF-ARW	Advanced Research version of the Weather Research and Forecasting (Model)
WSMR	White Sands Missile Range

<b><u>No. of Copies</u></b>	<b><u>Organization</u></b>
1 (PDF)	DEFENSE TECHNICAL INFORMATION CTR DTIC OCA
2 (PDFS)	DIRECTOR US ARMY RSRCH LAB RDRL CIO LL IMAL HRA RECORDS MGMT
1 (PDF)	GOVT PRINTG OFC A MALHOTRA
1 (PDFs)	DIRECTOR US ARMY RSRCH LAB J PASSNER

INTENTIONALLY LEFT BLANK.